PART II:

FOC

- FOC

Chapter 4
FOC Instrument Overview

In This Chapter...

The Faint Object Camera (FOC), desinged and built by the European Space Agency, is the highest-resolution imaging instrument on the Hubble Space Telescope (HST). It is a long focal-ratio, photon-counting imager operating in the 1150 to 6500 Å wavelength range with a 14 x 14 arcsecond field of view. The Corrective Optics Space Telescope Axial Replacement (COSTAR), installed during the December 1993 servicing mission, restored the two prime scientific objectives of the FOC—deep imagery and photometry of very faint celestial objects and imagery of bright objects at the highest possible resolution—which were hampered by the spherical aberration of the telescope's primary mirror. The corrected FOC offers imaging capabilities with a pixel size of 0.014" and a FWHM of 2–3 pixels, providing peak sensitivity at 3400 Å. Low detector background and insensitivity to cosmic rays allow for long exposures providing very deep photometry of point sources, reaching a S/N of 10 for a V = 26 B5V star in a 45 minute exposure.

Two cameras, named *f*/48 and *f*/96 after their original focal ratios, are available on the FOC, but difficulties with the *f*/48 camera have made the *f*/96 camera the FOC's workhorse, responsible for virtually all of the imaging. Since the installation of COSTAR, the *f*/48 camera has been used exclusively for long-slit spectroscopy. Observers should be aware that the names of these cameras no longer describe their actual focal ratios. COSTAR has raised the *f*/ratio of HST's Optical Telescope Assembly (OTA) from *f*/24 to *f*/37, increasing the *f*/number of the two FOC cameras from *f*/48 to *f*/75.5 and from *f*/96 to *f*/151. However, because

the original names are deeply rooted in the HST ground system at all levels, from proposal entry to data archiving, we have been forced to retain these names. Table 4.1 summarizes the post-COSTAR imaging characteristics of the FOC.

Table 4.1: Summary of FOC Performance Characteristics

Optical Modes	**f/48[a]**	**f/96**
Focal ratio	75.5	151
Operating range (Å)	1150–6500	1150–6500
Number of bandpass filters	11	39
Bandpass FWHM (Å) max	2700	2300
Bandpass FWHM (Å) min	300	34
Maximum ND attenuation (mag.)	0	9
Field of view (arcsec) max	28 x 28	14 x 14
Field of view (arcsec) min (128x128)	3.6 x 3.6	1.8 x 1.8
Unzoomed pixel size (arcsec)	0.029	0.014
Minimum wavelength for critical sampling (Å)	6500	3250
Peak efficiency (%)	6.6	7.9
Peak wavelength (Å)	3400	3700
Limiting magnitude, point source[b]	27	27.5
Limiting magnitude arcsec^{-2}, extended source[c]	23.5	23
Dynamic range, point source[d] (mag)	20–27	19–27.5
Dynamic range, extended source[e] (mag arcsec^{-2})	18–25	17–25
Overload magnitude	9	9
Number of polarizing prisms[f]	0	3

a. The *f*/48 mode has been available for long slit spectroscopy in Cycles 6 and 7.
b. S/N = 5, 5 hour integration, U band.
c. Same as b. over 0.1” x 0.1” area.
d. 2 counts sec^{-1} pixel^{-1} upper limit.
e. 0.5 counts sec^{-1} pixel^{-1} upper limit.
f. 0 degrees, 60 degrees, 120 degrees direction of polarization.

4.1 Spatial Resolution and PSF

COSTAR has restored many of the FOC’s envisioned capabilities, in that the COSTAR-corrected PSF contains more than 75% of the visible light within a radius of 0.1 arcsecond, while losing less than 20% of the light to the two reflections at the two extra mirror surfaces. The net increase in sensitivity is a

factor of approximately 3-4 at visible wavelengths. COSTAR's improvement of the FOC PSF is illustrated in Figure 4.1, which shows the radial profile of an aberrated PSF image and a COSTAR-corrected image at 4860Å. Archive users should consult the *FOC Instrument Handbook*, version 3.0 for more details on the pre-COSTAR characteristics of the FOC.

Figure 4.1: PSF Before and After COSTAR

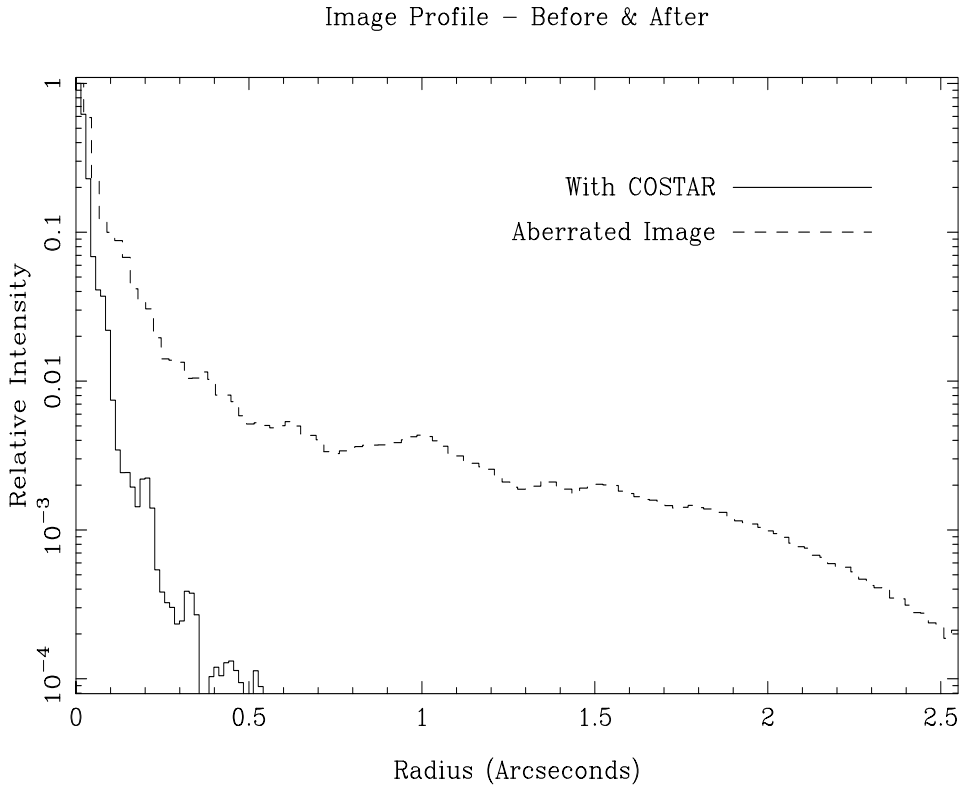

The encircled energy fraction $\varepsilon(\lambda)$ is tabulated in the *FOC Instrument Handbook*, version 7.0 (Table 9) for various circular apertures. This quantity is normalized so that the encircled energy is 1.0 at a radius of 1 arcsecond (70 pixels). Figure 4.2 compares the encircled energy curves of the aberrated OTA, the COSTAR-corrected OTA, and a perfect diffraction-limited image from a 2.4m circular aperture with a 0.33 central obstruction, showing that the COSTAR-corrected FOC PSF approaches that of an ideal imaging system in both encircled energy performance and in the FWHM of the PSF core.

Figure 4.2: Encircled Energy Fraction and PSF Profile Before and After COSTAR

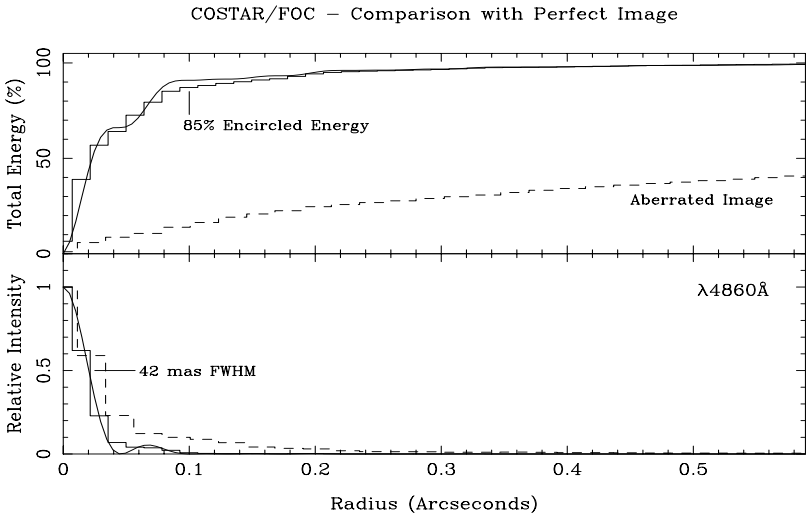

4.2 Filters

The FOC has six commandable rotating filter wheels holding 58 optical elements and six clear apertures. Four wheels are on the *f*/96 camera, and two are on the *f*/48 camera. The filter wheels of the *f*/96 camera have long pass, wide band, medium band, narrow band and neutral density filters. They also contain three polarizers and two objective prisms. The filter wheels of the *f*/48 camera contain long pass, wide band, and three objective prisms. Tables 3 and 4 of the *FOC Instrument Handbook*, version 7.0, gives a complete list of the optical elements ordered by increasing peak wavelengths and provides information on their transmission and wavelength coverage. This table also lists the magnitudes of attenuation of the neutral density filters, which can diminish the beam in increments of one magnitude from one to nine magnitudes.

4.3 Formats & Fields of View

The FOC *f*/96 camera has a maximum field of view of 14 x 14 arcseconds square, obtained with the 512 x 1024 zoomed format, although the dynamic range of this format is limited. The FOC can operate with normal pixels (square, 25 x 25 microns) or zoomed pixels (rectangular, 50 x 25 microns). Normal pixels provide a plate scale of 0.01435 arcsec pixel^{-1} for the *f*/96 camera, and 0.02870 arcsec pixel^{-1} for the *f*/48 camera. Zoomed pixels are twice as long in the *x* direction. All formats larger than 512 x 512 pixels automatically have an 8-bit word length. Table 4.2 and Table 4.3 provide the main characteristics of the standard formats for the *f*/96 and *f*/48 camera respectively, where the first column gives the format size (S x L), the second the pixel size in microns, the third the starting point in

pixels, the fourth the word length, the fifth the zoom configuration, and the sixth the overall field of view in arcseconds squared for that format.

Table 4.2: Available f/96 Formats

Format (S x L)	Pixel Size (μm^2) ($arcsec^2$)	Offset (S_0,L_o)	Word Length	Zoom	FOV ($arcsec^2$)
512 x 1024	50 x 25 (0.029 x 0.014)	0,0	8 bit	on	14 x 14
512 x 1024	25 x 25 (0.014 × 0.014)	256,0	" "	off	7 x 14
512 x 512	50 x 25 (0.029 x 0.014)	0,256	16 bit	on	14 x 7
512 x 512	25 x 25 (0.014 x 0.014)	256,256	" "	off	7 x 7
256 x 256	" "	384,384	" "	" "	3.6 x 3.6
128 x 128	" "	448,448	" "	" "	1.8 x 1.8

Table 4.3: Available f/48 Formats

Format (S x L)	Pixel Size (μm^2)	Offset (S_0,L_o)	Word Length	Zoom	FOV
512 x 1024 (imaging)	50 x 25 (0.057" x 0.029")	0,0	8 bit	on	28" x 28"
512 x 1024 (spec)	50 x 25 (0.057" x 1.7Å)	0,0	8 bit	on	28" x 1700Å
512 x 1024 (spec)	25 x 25 (0.029" x 1.7Å)	192,0	8 bit	off	14" x 1700Å
256 x 1024 (spec)	25 x 25 (0.029" x 1.7Å)	320,0	16 bit	off	7" x 1700Å

4.4 Sensitivity

The overall (OTA + COSTAR + FOC) central absolute quantum efficiency in counts $photon^{-1}$ with no filters in the beam is plotted and tabulated as a function of wavelength in Figure 4.3 (and also Table 11 of the *FOC Instrument Handbook*, version 7.0), for the four FOC imaging and spectrographic configurations. The data represent the product of in-orbit measurements for the *f*/96 relay+OTA absolute quantum efficiency, and ground-based reflectance calibrations of the COSTAR mirrors for the *f*/48. The predicted loss of light from two reflections of MgF_2 coated aluminum COSTAR mirrors amounts to a 20% loss in the visible and a 35% loss in the ultraviolet. The loss due to the COSTAR mirrors is more than compensated by the improvement in image quality, because the encircled

energy performance within a 0.1” radius has improved from 18% to ≅80% within the same area.

Figure 4.3: Baseline Overall Quantum Efficiency.

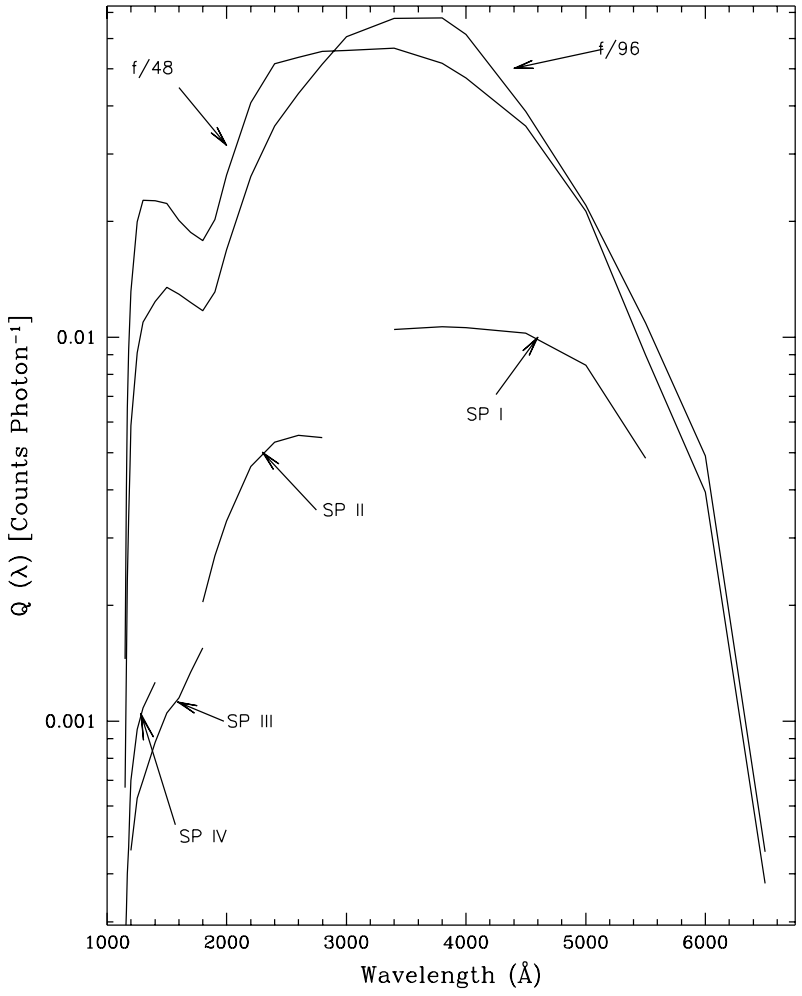

4.5 Polarization & Spectroscopy

In addition to standard imaging, the FOC can also perform polarization imaging, objective prism spectroscopy, and long-slit spectroscopy.

- Three polarizer filters available on the *f*/96 camera, with pass directions of 0 degrees, 60 degrees and 120 degrees, provide a straight-through, low reflection-angle system which introduces less than 2% intrinsic polarization.
- Two objective prism filters on the *f*/96 camera allow observers to obtain high-throughput spectra at low to medium resolution from 1700Å to 6000Å (near-UV prism) and 1150Å to 6000Å (far-UV prism).

- The *f*/48 camera possesses a long-slit spectroscopy facility with a resolving power of ~1150 in 4 orders, covering 3600–5400 Å, 1800–2700 Å, 1200–1800Å, and 1150–1350 Å.

4.6 What to Expect

This section highlights some typical FOC image characteristics. Rather than trying to present examples of every possible mode, we focus on the *f*/96 imaging mode, because it is the most commonly used. Examples of *f*/48 images, *f*/48 longslit spectra, and prism images appear in later sections.

Keep in mind that the grayscale representations used in this manual seldom highlight the subtleties of the data. There is no substitute for actually displaying the data on a monitor.

Some images in this section are displayed with higher intensities as white and lower intensities as black (positive), other images are displayed the opposite way (negative).

Commonly Observed Features

If your FOC data are well-exposed, you might see one or more of the following:

- Occulting fingers located near the aperture entrance if the image size is greater than 512 x 512 pixels or if the FUV prism is in the beam.
- Reseau marks etched onto the faceplate of the detector to aid in geometric correction (Figure 4.4).
- Blemishes (scratches on the faceplate, Figure 4.4).
- Vertical intensity variations along the right edge of the image (due to a variation in camera scan speed).
- A faint diagonal parallel striping pattern called *pattern noise*.

After geometric correction your images may additionally show:

- A very faint moiré pattern (“thumbprint”), which is a variation of the noise, *not the signal*, caused by the geometric correction (Figure 4.5).
- Warped edges (Figure 4.4).

These features are all normal and should be expected. They can be traced either to the instrumental design and performance of the FOC or the calibration process which corrects for geometric distortion.

Figure 4.4: FOC f/96 Image of an Extended Source

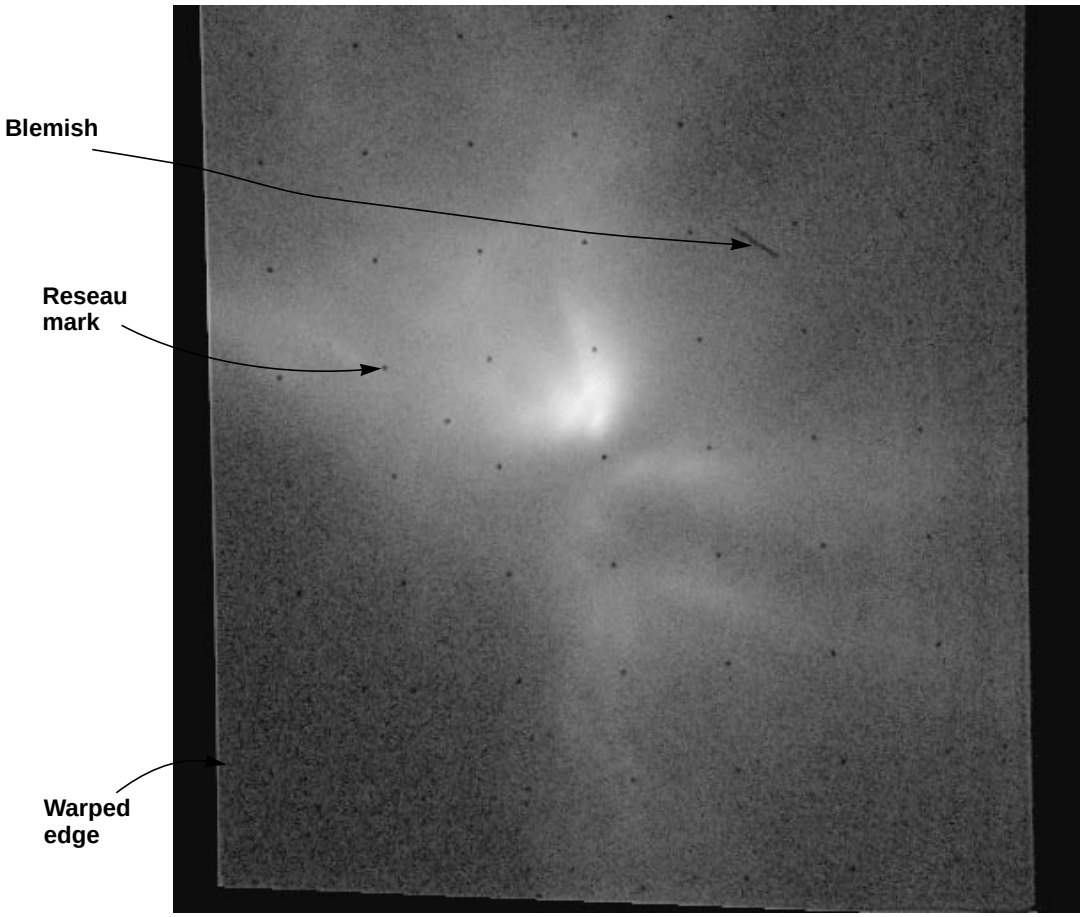

Figure 4.4 is a positive rendition of an *f*/96 (F430W) 512 x 512 image of the reflection nebula LK-H alpha 233. The image has been fully calibrated by the FOC pipeline and shows features that are common in any well-exposed FOC image. The regular grid of reseau spots are used for geometric distortion calibration. The warped edges are produced by the pipeline during the geometric transformation. A blemish is seen above and to the right of center.

Figure 4.5: FOC 512x512 Image Showing Faint “Thumbprint” Pattern or “Fringes”

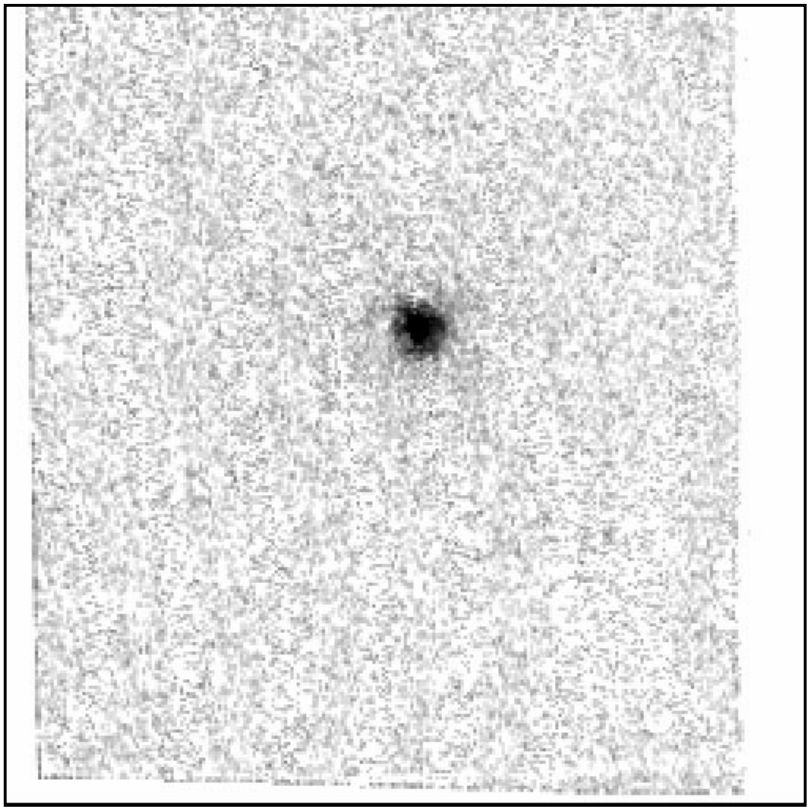

Images that have been geometrically corrected often show the pattern evident in the above grayscale picture: a thumbprint pattern at low intensity levels. It is quite hard to see, appearing most clearly when the image has a low (~1 count per pixel or so) spatially flat background. The thumbprint pattern is a modulation of the local noise characteristics of the data, not of the intensities themselves. It is a by-product of the geometric correction process in which the raw (geometrically distorted) image is resampled with an interpolator that takes a weighted mean of the four nearest pixels to determine the geometrically corrected pixel value (see “Geometric Correction (GEOCORR)” on page 6-5 for details). The weightings vary smoothly with position in the image, such that at some places, a single pixel dominates the weightings (the noise of the resampled pixel is the same as that of the original data), while at other places the weightings favor all four pixels equally (the average noise is half of the noise of the individual pixels). The fringes are contours of constant weighting.

The actual pattern depends on the particular geometric correction file used, and thus depends on the format. The effect on the scientific utility of the data is minimal, unless one requires accurate values of the noise per pixel for each pixel.

Figure 4.6: Full-Format f/96 Image of a Bright Extended Source

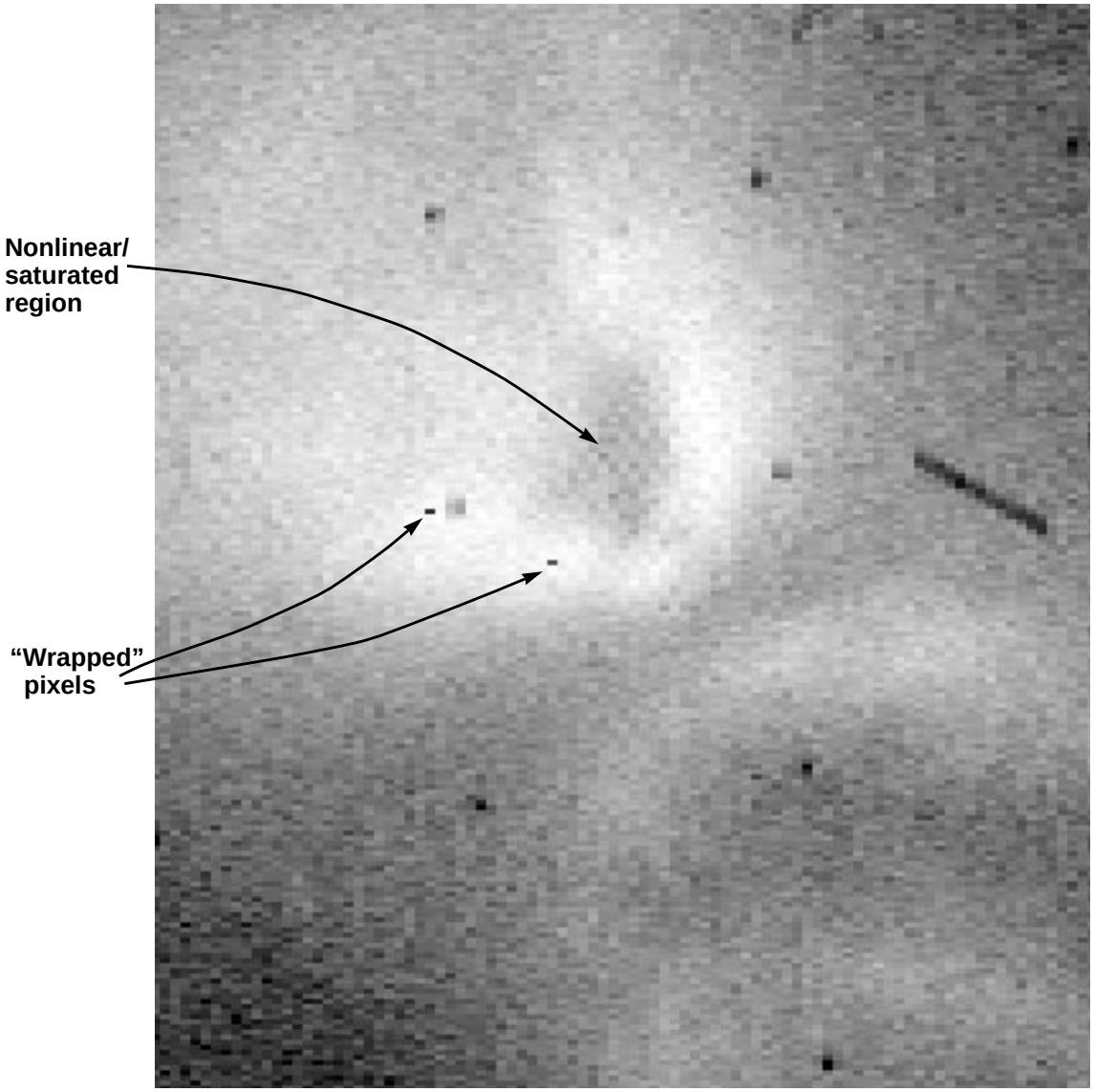

The portion of a full-format *f*/96 image shown above illustrates 8-bit wrapover and saturation. The former occurs when the image format selected is 512 x 1024 (zoomed or unzoomed). In that case, the image memory is configured so that there are only 8 bits per pixel. The maximum pixel intensity in raw full-format data is therefore only 255 counts; a further detected photon in a pixel causes the recorded intensity to cycle back to zero. After dezooming a full-format image, the maximum pixel intensity in the raw data is 255/2 = 127.5. The two pixels indicated have suffered from wrapover—they appear as rectangular because the raw dezoomed image is displayed. The dark region is an area where the photon count rate is higher than the FOC can count without suffering coincidence losses.

Chapter 5
FOC Data Structures

In This Chapter...

When newly-gathered HST data arrive at STScI, a system known as OPUS[1] immediately partitions the data into separate files, looks for discrepancies between the planned and executed observations, calibrates the data files, and deposits them in the HST Archive. The FOC data files you obtain from the Archive via the Internet or on a data tape will be in FITS format. Before you analyze these data, you will want to convert them to GEIS format. The names of the resulting GEIS files will consist of a nine-character rootname, whose syntax is explained in Appendix B, and a three-character suffix. Chapter 2 describes the GEIS and FITS file formats, and shows how to convert archival FITS files into GEIS files. This chapter describes how these FOC data files are organized, including:

- The contents of files corresponding to each three-letter suffix.
- The keywords contained in FOC file headers.
- The relationship between the data and the original Phase II proposal request.
- The paper products associated with each dataset.

5.1 File Suffixes

The name of each file in an FOC dataset, such as `x3l80101t.d0h`, has a three-character suffix, in this case the `d0h`, that uniquely identifies the file's content. When an FOC image comes down from the telescope, it is stored in files

1. OSS and PODPS Unified System (OPUS).

with suffixes .d0h/.d0d. The image is then automatically calibrated to produce the .c0h/.c0d and .c1h/.c1d files. The .c1h/.c1d files contain the final calibrated data, which are likely to be of greatest interest to observers. Table 5.1 gives the various file suffixes for the FOC and the corresponding file contents, listing all of the files that the pipeline can produce. Not all of the processing steps are performed for every observing mode, so only a subset of these files may be available.

In addition to the image files, the .trl or *trailer* file—which comes with each FOC observation—is an ASCII text file that describes the standard processing applied to the images by OPUS. The .pdq file reports any real-time activities associated with the observation, such as slews for an interactive acquisition, and any problems that might have occurred with the telescope, such as a guide star acquisition failure or guide star recenterings. The standard header packet (.shh and .shd files) contains information about the scheduling of the observation. The data quality files (.q0h and .q0d), in principle, would contain information on position of blemishes in FOC images. However, they are not used by the FOC because these positions vary with time, limiting the utility of these files. The unique data log files (.ulh and .uld) contain engineering information not generally of interest to most observers.

Table 5.1: FOC Dataset Suffixes

Suffixes	File Contents
Raw Data Files	
.d0h/.d0d	Raw science data
.q0h/.q0d	Data quality for raw science data
.shh/.shd	Standard header packet containing observation parameters
.ulh/.uld	Unique data log
Calibrated Data Files	
.c0h/.c0d	dezoomed, geometrically corrected data, with photometry
.c1h/.c1d	All of the above, plus flatfielded data
.trl	Trailer file
.pdq	Post Observation Summary and Data Quality Comment file

5.2 Header Keywords

FOC image headers contain numerous keywords specifying how an observation was taken and how the resulting data were calibrated. The following keywords in the .c1h header file describe the instrumental setup of the FOC during the observation:

- Configuration or optical relay (OPTCRLY): *f*/96 or *f*/48.
- Filters employed (FILTNAM*).
- Spectrographic mirror position (SMMMODE).
- Image size (SAMPPLN and LINEPFM).
- Position of starting pixel on photocathode (SAMPOFF and LINEOFF).
- Pixel size (PXFORMT): normal or zoomed.
- Reference pixel in the chosen format (CRPIX1 and CRPIX2).

For easy reference, Table 5.2 lists these header keywords, their definitions, and the possible keyword values for the commonly used FOC observing modes.

The quickest way to learn how each observation was actually performed is to use the **iminfo** task in the STSDAS **toolbox.headers** package. This task provides a user-friendly synopsis of the most relevant header information, extracted from the ASCII header and the group parameters in the binary data file. Figure 5.1 shows sample results of running **iminfo** on the final calibrated data file for an FOC image. Included in the listing are the target name, target RA and Dec, observation date, exposure time, basic image statistics, basic instrument configuration, basic observing mode, the calibration steps performed, and the number of groups in the image (only one for the FOC).

Figure 5.1: FOC iminfo Output

```
Rootname            Instrument              Target Name
X2X10108T              FOC                  BPM16274

Program         = 2X1                 Obs Date        =  6/10/95
Observation set = 01                  Proposal ID     = 06160
Observation     = 08                  Exposure ID     = 01-023
Source          = Tape Recorded       Right ascension =   0:50:03.2
File Type       = SCI                 Declination     = -52:08:17
                                      Equinox         = J2000

Naxis1 = 256            Datamin = 0.                  Number of groups = 1
Naxis2 = 256            Datamax = 1454.249            Parameters/group = 18

Configuration   = f/96
Image format    = NORMAL                        Image orientation = -35.0
Shutter mode    = NOTUSED                       Exposure time     =  722.4
LED calibration = NOTUSED                       Sample begin      = 385
LED color       =                               Line begin        = 385
Coronographic apodizer = NOTUSED                Bits/data number  = 16
Spectrographic mirror  = NOTUSED                Calibration steps completed:
Filter names: F4ND, CLEAR2, CLEAR3, F253M           UNI  WAV  GEO
he>
```

To see the full list of header keywords, you can invoke the IRAF **imheader** task by typing, for example:

```
cl> imheader x2x10108t.c1h long+ | page
```

These additional keywords provide information on such things as the photometric transformation of the image, any interruptions of the exposure, and the guidance mode used during the observation. Some of the more critical keywords are listed in Table 5.2, grouped by the type of information they provide.

The values of the target keywords are extracted from the proposal prior to execution, with the orientation keyword ORIENTAT providing the angle between North and the image's *y* axis. The exposure keywords, on the other hand, describe the actual execution of the observation. For example, if a problem interrupted the exposure, the EXPFLAG keyword would report this condition. After the observation has been taken, standard processing supplies information on the filters, format, and optical relay used for the image. The PHOTMODE keyword concisely summarizes the image configuration, and the inverse sensitivity keyword PHOTFLAM gives the factor which converts count rates to flux units (see Chapter 3 for more on HST photometry keywords).

FOC images taken after mid-November 1993 contain the KX_DEPLOY keyword in their headers. This keyword has the value "T" if COSTAR is deployed and "F" otherwise. Before November 1993, the KX_DEPLOY keyword did not exist, but in most cases the name of the data file itself will tell you whether the image is aberrated. Rootnames of observations taken prior to the December 1993 servicing mission begin with `x0` or `x1`, while FOC images taken after the servicing mission begin with `x2`, `x3`, or `x4` and benefit from COSTAR correction. A small number of images were taken after the first servicing mission but before COSTAR deployment; however, these were generally uninteresting calibration images.

Images that begin with `x0` or `x1` are pre-COSTAR (i.e., the PSF is spherically aberrated).

Table 5.2: FOC Header Keywords

Keyword	Definition	Possible Values
	Image Format	
OPTCRLY	Optical relay used	F48 or F96
KX_DEPLOY	Was COSTAR deployed for FOC? (only for images taken after 11/20/93)	T or F
CAMMODE	Coronographic optical mode. This keyword indicates whether or not the coronographic apodizing optics are inserted in the *f*/96 beam. If so, the effective focal ratio becomes *f*/288. It applies only when OPTCRLY=F96.	NOTUSED (normal *f*/96 mode) or INBEAM (*f*/288 coronographic mode)
SMMMODE	Spectrograph mirror mechanism mode. This keyword indicates whether or not the spectrograph relay mirror is inserted into the *f*/48 beam to redirect the light to the grating. It applies only when OPTCRLY=F48.	NOTUSED (normal *f*/48 mode) or INBEAM (spectrographic mode)
SHTMODE	Shutter mode. Indicates whether the shutter is closed (as would be expected for dark exposures or LED flatfields).	NOTUSED (shutter open) or INBEAM (shutter closed)

Table 5.2: FOC Header Keywords (Continued)

Keyword	Definition	Possible Values
LEDMODE	LED mode. Indicates whether one of the internal calibration flatfield sources is on.	NOTUSED (LED off) or ACTIVE (LED on)
SAMPPLN	Number of pixels per scan line (number of pixels along *x* axis).	512, 256, 128, or 64
LINEPFM	Number of scan lines per frame (number of pixels along *y* axis).	1024, 512, 256, 128, or 64
SAMPOFF	*x* offset of 0,0 pixel in frame.	From 0 to 1023,75 in 0.25 increments
LINEOFF	*y* offset of 0,0 pixel in frame.	From 0 to 1023.75 in 0.25 increments
PXFORMT	Pixel format. NORMAL indicates square pixels, ZOOM indicates rectangular pixels (2x1).	NORMAL or ZOOM
DNFORMT	Number of bits per pixel.	8 or 16
	Exposure Information	
DATE-OBS	UT Calendar Date Observation was taken	DD/MM/YY
TIME-OBS	UT at start of observation	HH:MM:SS
EXPTIME	Exposure time	Duration of exposure in seconds
EXPFLAG	Flag to indicate whether the exposure was interrupted as a result of telescope problems	NORMAL (if no interruptions) or INTERRUPTED
FILTNAM1	Filter element name for wheel 1.	***f/96:*** CLEAR1, F600M, F630M, F2ND, F4ND, F6ND, F8ND, PRISM1, PRISM2, POL0, POL60, POL120 ***f/48:*** CLEAR1, F140W, F150W, F175W, F195W, F220W, F305LP, PRISM3
FILTNAM2	Filter element name for wheel 2	***f/96:*** CLEAR2, F140W, F175W, F220W, F275W, F320W, F342W, F430W, F370LP, F486N, F501N, F480LP ***f/48:*** CLEAR2, F275W, F130LP, F180LP, F342W, F430W, PRISM1, PRISM2
FILTNAM3	Filter element name for wheel 3	***f/96:*** CLEAR3, F120M, F130M, F140M, F152M, F165W, F170M, F195W, F190M, F210M, F231M, F1ND ***f/48:*** Left blank
FILTNAM4	Filter element name for wheel 4	f/96: CLEAR4, F253M, F278M, F307M, F130LP, F346M, F372M, F410M, F437M, F470M, F502M, F550M f/48: Left blank

Table 5.2: FOC Header Keywords (Continued)

Keyword	Definition	Possible Values
	Target Information	
TARGNAME	First 10 characters of the target name as given in proposal	
ORIENTAT	Image Orientation	-180 to 180 degrees
CRVAL1	Right Ascension of the reference pixel	(RA in degrees)
CRVAL2	Declination of the reference pixel	(Dec in degrees)
CRPIX1	*x* position of the reference pixel	468 in a 1024x1024 f/96 image 512 in a 1024X1024 f/48 image
CRPIX2	*y* position of the reference pixel	537 in a 1024X1024 f/96 image 512 in a 1024X1024 f/48 image
Photometry Keywords		
PHOTMODE	Observation mode specified by the relay used (OPTCRLY), the format, and the filters in place.	e.g., 'FOC F/96 COSTAR F220W X96N512'
PHOTFLAM	Inverse sensitivity; conversion factor from counts sec^{-1} to ergs cm^{-2} sec^{-1} $Å^{-1}$; a star with this flux would have a total of 1 count/sec within a 1" radius.	
PHOTZPT	Zero-point of the ST magnitude system	-21.10
Calibration Information (See Chapter XX for more details)		
GEOCORR	Describes whether the geometric correction has been applied	COMPLETE, OMIT
PXLCORR	Describes whether pixels were dezoomed	COMPLETE, OMIT
UNICORR	States whether the flatfield correction has been applied	COMPLETE, OMIT
WAVCORR	States whether the photometric conversion has been calculated	COMPLETE, OMIT
BACCORR	Specifies state of background subtraction	COMPLETE, OMIT
ITFCORR	Specifies state of format-dependent photometric correction	COMPLETE, OMIT
SDECORR	States whether the spectrographic detector efficiency correction was applied	COMPLETE, OMIT

An HST Keyword Dictionary is available via the world wide web at:

`http://archive.stsci.edu/keyword/`

The dictionary gives more complete definitions of all keywords and all file types (e.g., science data files, standard header packets, unique data logs) for each of the HST instruments.

5.3 Relationship to Proposed Observations

Observers should recognize that their observations do not necessarily execute in the order listed in their Phase II proposals, but rather are scheduled so that they maximize the overall efficiency of HST. The first step in understanding how your data files relate to your original request is to examine the header keywords using **iminfo** or **imheader**. For example, the **iminfo** listing in Figure 5.1 says that exposure `x2x10108t` was a 722.4 second exposure of target BPM16274 using filters F253M+F4ND with the 256 x 256 format of the *f*/96 camera. It also gives the Exposure ID as 01-023, meaning the exposure listed under Visit 1, Exposure Logsheet line 23 of the Phase II proposal.

To see how the actual observation compares with the corresponding request, you can retrieve recent proposals via the HST Proposal Information Page at:

`http://presto.stsci.edu/public/propinfo.html`

Simply enter the Program ID (or proposal number; 6160 in the example above) into the box, click on the “Get Program Information” box and select either the full text or the formatted listing. Figure 5.2 shows an example of the formatted listing for the proposal at hand. Examination of this exposure logsheet shows that Line 23, Visit 1, requested one 423s exposure of BPM16274 using the F253M+F4ND filters and the 256 x 256 format of the *f*/96 camera. The EXPAND requirement increased the exposure time to fill the rest of the visibility period.

For Cycle 4 and earlier programs, the Exposure ID field reflected the use of RPSS instead of RPS2 for proposal submission. Entries in these Exposure ID fields look something like 23.000000, which means the exposure that corresponds to Exposure Logsheet Line 23. Where several exposures come from the same Exposure Logsheet line (e.g., if a spatial scan is used, or the Number_of_Iterations keyword is more than 1), the Exposure ID field contains a number like 23.0000000#001, to signify the first exposure corresponding to Exposure Logsheet line 23.

You may notice that the requested and actual exposure times differ for external FOC observations, even when no EXPAND requirement is specified. This disparity arises because the flight software that controls the FOC contains a bug that shortens the length of an exposure by approximately 3.5–4.5 seconds. Because typical FOC exposures last much longer than 4 seconds and the science header reports the correct exposure time, rewriting the software to correct the bug was deemed unnecessary.

Figure 5.2: Exposure Logsheet Via World Wide Web

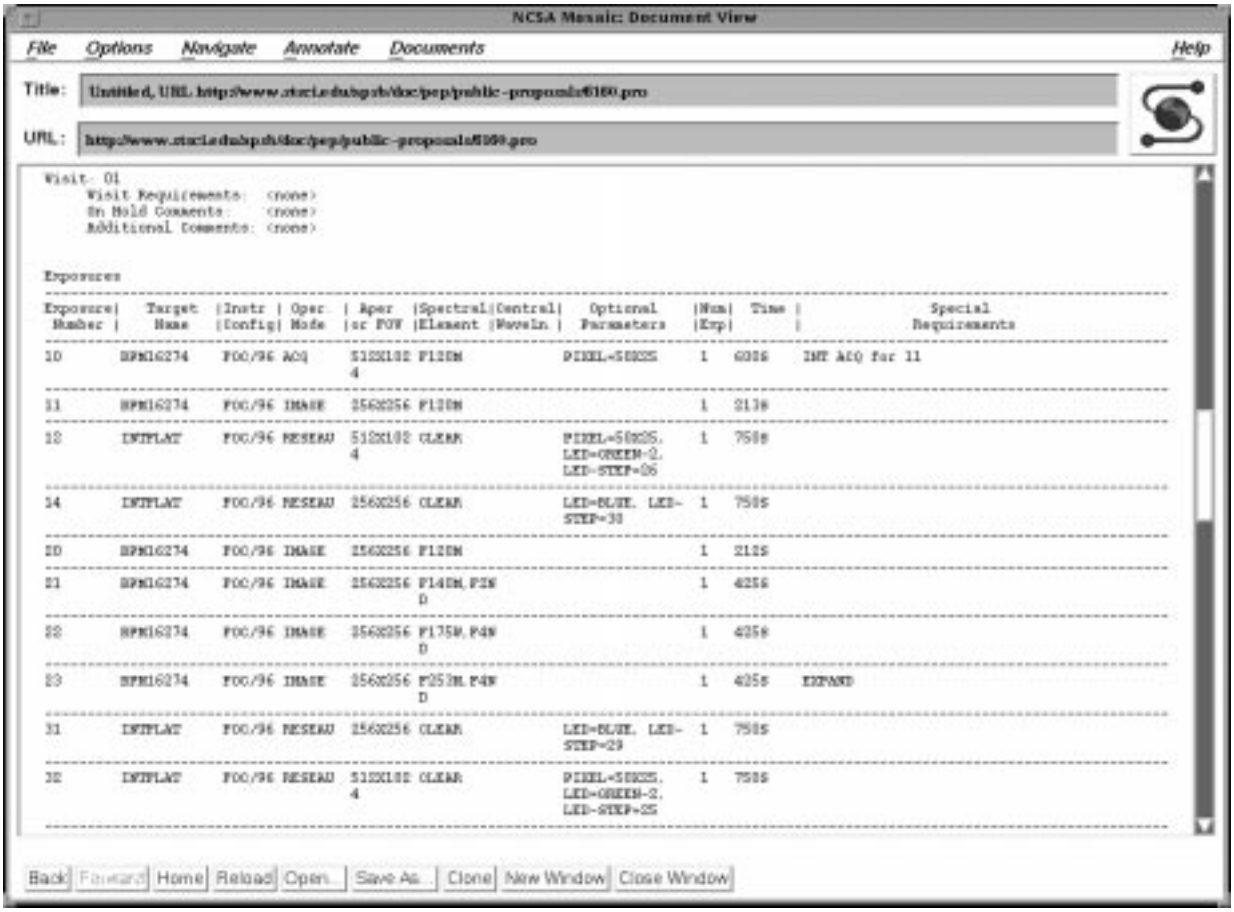

Having matched the exposure logsheet lines to the data received, you then need to determine whether the exposure proceeded normally. The most important resource for assessing potential problems is the PDQ file (see Chapter 2), a text file created by OPUS that records information about the state of the observatory during the observation, along with any processing abnormalities. It reports ptoential problems in the free-form comment fields QUALITY, QUALCOM1, QUALCOM2, and QUALCOM 3, as well at the end of the file. Figure 5.3 gives an example of such a report.

Figure 5.3: PDQ File for an FOC Exposure

xterm

```
---------- Post Observation Summary and Data Quality Comments (PDQ) ----------

DATASET = 'X2X10108T'
Proposal Id: 06160                                                  dd/mm/yy
Principal Investigator  : JEDRZEJEWSKI, ROBERT                Date: 06/10/95

Target Name    : BPM16274
Target RA (hms):   0 50  3.180         Target Dec (dms): -52  8 17.400

Actual Start Time of Observation : 6/10/95  08:18:54 UT
Calib. Type (Int/Ext/ ):                 Calibration Flag (Y/N) : Y
Operating Mode : IMAGE                   Aperture : XK96N256

-------------------------- Data Quality Evaluation: --------------------------
QUALITY = 'POOR'
QUALCOM1= 'BPM16274, target star near center of image'
QUALCOM2= 'guide star acquisition failed to single star fine lock'
QUALDATE= ' 7-OCT-1995 00:49'

----------------------- Observation Characteristics: -------------------------

  -- PLANNED characteristics of FOC   exposure from SHH file --
Filters 1 2 3 4 : 7              0              0              8
Optical Relay   : F96                     Image Format        : NORMAL
Spectrographic Mirror Mechanism: NOTUSED    Shutter Mode        : NOTUSED
LED Calibration Status         : NOTUSED    Coronogr. Apod. Mask: NOTUSED
Sample offset                  :  384.00    Line offset         :  384.00
Commanded exposure duration (sec) :    726.00

   -- ACTUAL characteristics of FOC   exposure from D0H file --
Filter names    : F4ND          CLEAR2        CLEAR3        F253M
Filters 1 2 3 4 : 7              0              0              8
Optical Relay   : F96                     Image Format        : NORMAL
Spectrographic Mirror Mechanism: NOTUSED    Shutter Mode        : NOTUSED
LED Calibration Status         : NOTUSED    Coronogr. Apod. Mask: NOTUSED
Sample offset                  :  384.00    Line offset         :  384.00
Actual exposure duration (sec) :       722.38

---------------------------- D0H Data Structure: ----------------------------
D0H File Group Count: 1              DCF fill: 0         Axis 1 length: 256
                                   PODPS fill: 0         Axis 2 length: 256

------------------------- Observation Statistics: ---------------------------

           ####################  PODPS IMAGE STATISTICS  ###################
> #               IMAGE      NPIX      MEAN     STDDEV     MIDPT       MIN
MAX
    x2x10108t.c0h[1]     65536    0.6888     10.43     0.623        0.     1454
.
> #               IMAGE      NPIX      MEAN     STDDEV     MIDPT       MIN
MAX
    x2x10108t.c1h[1]     65536    0.6789     10.43    0.6173        0.     1454
.


------------------------------- Extracted OMS Keywords: ----------------------

GUIDECMD= 'FINE LOCK           '/ Commanded Guiding mode
GUIDEACT= 'FINE LOCK/GYRO      '/ Actual Guiding mode at end of GS acquisition
NLOSSES =                    0 / Number of loss of lock events
LOCKLOSS=                  0.0 / Total loss of lock time (sec)
NRECENT =                    0 / Number of recentering events
RECENTR =                  0.0 / Total recentering time (sec)
V2_RMS  =                  2.0 / V2 Axis RMS (milli-arcsec)
V2_P2P  =                 14.8 / V2 Axis peak to peak (milli-arcsec)
V3_RMS  =                  2.7 / V3 Axis RMS (milli-arcsec)
V3_P2P  =                 53.2 / V3 Axis peak to peak (milli-arcsec)
GSFAIL  = '            DEGRADED'/ Guide star acquisition failure!

-------------------------------  Additional Comments: ------------------------

The guide star acquisition at 04:32 failed to single-star fine lock with FGS 1
(HSTAR 5326). As a result there could be some roll about the guide star in
FGS 1, but a comparison of the first and last images of the target after the
offsets were uplinked, shows that the motion was no more than about 0.05
arcsec. Observation X2X10102 was taken before the offsets could be uplinked,
and as a result is blank. The offsets of dV2= -4.1, dV3= -1.7 were uplinked
at 06:33. Observations X2X10104-0A were taken after the maneuver. The TM_GAP
keyword in the JIH file is wrong for internal exposures 03, 04, 09, and 0A.
It should be 0 seconds.

he>
```

Items to look for are:

1. Was the FGS guiding mode the same as was requested?

   The default guide mode for FOC observations is fine lock. If the guide star acquisition fails, it is possible to default to single-star guiding. In most cases, the effect on data quality is so small as to be unnoticeable. In the extracted OMS keywords section at the end of the PDQ file the keywords GUIDECMD and GUIDEACT should both be set to “FINE LOC”.

2. Were there any losses of lock or recenterings?

   These glitches can degrade an observation slightly, although again the effect is small. Look at the OMS keywords NLOSSES and NRECENT.

3. Were there any data dropouts?

   The DCF fill and PODPS fill parameters in the `.d0h` data structure section should both be zero.

4. Were there any instrument anomalies?

   If the OPUS examination of the data detected any suspicious artifacts that might signify an instrumental problem, a comment will appear in one of the QUALCOM keywords, perhaps with some expansion in the “Additional Comments” section at the end.

5. Were there any small-angle maneuvers executed by the telescope?

   Such would be the case if an exposure were preceded by an Interactive Acquisition. If so, there will generally be an observer comments (`.ocx`) file giving the details of any such moves, and OPUS staff usually record the moves in the comments section at the end of every affected observation

5.4 Paper Products

All HST observers currently receive a set of Paper Products shortly after a given observation executes. These documents provide a quick first look at the data, summarize the image statistics, and point out potential problems with the data, drawing on information in the PDQ file. All observers, including Archive users, can run the **pp_dads** task in STSDAS to obtain a set of paper products for any FOC dataset. To receive a full report, you will need the following files: `.d0h/.d0d`, `.c0h/.c0d`, `.c1h/.c1d`, `.shh/.shd`, `.jih/.jit`, `.pdq`. See the STSDAS on-line help for details (type `help pp_dads`).

The FOC paper products were recently redesigned to enhance their clarity and usefulness. The first several pages provide a general description of the visit, and each individual exposure generates two additional pages of information. One displays a greyscale plot of the image and its orientation, along with the exposure time and basic instrument configuration. The other summarizes the spacecraft performance during the observation, the calibration status, and any anomalies flagged in the PDQ file. (See Figure 5.4 through Figure 5.8 for examples.)

Figure 5.4: Explanatory Notes

FOC

Description of Visit Summaries

Target List

The Target List contains the target name, the coordinates for the target as calculated by the ground system based on the target information taken from the proposal, and the text description of the target given in the proposal. Note that the coordinates listed represent the predicted position of the target in the sky and do not give the pointing of HST at the time of the observation.

Observation List with Data Quality Flags

The Observation List contains information that uniquely identifies individual exposures as specified in the observing proposal. Additionally, the status of the spacecraft and ground-system performance during the execution of the observation are summarized by the Procedural Quality Flags:

OBS	Status of the performance of HST.
PROC	Status of the pipeline processing of the observations.
CAL	Status of the reference data used in calibration.

Symbols used to indicate the status of the Procedural Quality are:

○	OK.
●	Not OK-Refer to the Data Quality Summary for details.
Blank	Status unknown.

Observation Statistics

The Observation Statistics sections contains information about the modal count and count rate (determined by a 3-sigma clipping algorithm), and the maximum count and count rate.

Description of Exposure Summaries

Plots for Each Exposure

Plots are created for each exposure. Gray-scale or line plots are produced as appropriate for the instrument configuration and observing mode for each exposure. Exposure information taken from the headers of the data files is also provided.

HST Spacecraft Performance Summary for Each Exposure

The Data Quality Summary contains details of problems flagged by the Data Quality flags. Exposure information taken from the headers of the data files is also provided.

Pipeline Processing and Calibration Data Quality Summary for Each Exposure

The calibration summary gives detailed information about the calibration of the observations. Individual calibration steps are listed with completion status. Reference files used are listed by name and information about the pedigree of the calibration data is provided.

Need Help?

Send e-mail to your contact scientist or help@stsci.edu

Space Telescope Science Institute, Fri 14:22:42 12-Sep-97

Figure 5.5: Target and Observation Lists

Visit: 01 **Proposal: 06930** *FOC*

Target List

Target Name	R.A. (J2000)	Dec. (J2000)	Description
NGC5139	13:26:45.90	-47:28:36.7	Calibration
INTFLAT	0:00:00.00	0:00:00.0	(N/A)
DARK	0:00:00.00	0:00:00.0	(N/A)

Observation List

Logsheet Line#	Rootname	Target Name	Config.	Image Format	Filters	Exposure (sec)	Quality Flags Obs	Proc	Cal
1.010	X3YU0101M	NGC5139	FOC/96	512X512	F2ND,F470M	1097.12	○		○
1.020	X3YU0102M	NGC5139	FOC/96	512X512	F1ND,F470M	1282.12	○		○
1.025	X3YU0103M	INTFLAT	FOC/96	512X1024z	CLEAR	600.00	○		
1.026	X3YU0104M	DARK	FOC/96	512X512	F470M	600.00	○		
1.030	X3YU0105M	NGC5139	FOC/96	512X512	F470M	597.12	○		
1.040	X3YU0106N	NGC5139	FOC/96	512X512	F4ND,F470M	2094.12	○		
1.045	X3YU0107N	INTFLAT	FOC/96	512X1024z	CLEAR	600.00	○		
1.046	X3YU0108N	DARK	FOC/96	512X512	F6ND,F470M	600.00	○		
1.050	X3YU0109N	NGC5139	FOC/96	512X512	F6ND,F470M	2877.12	○		

Quality flags: ○ = OK ● = Not OK Blank = Unknown or file missing

Figure 5.6: Observation Statistics

Visit: 01 **Proposal: 06930** *FOC*

Observation Statistics

Logsheet Line#	Rootname	Target Name	Image Format	Exposure (sec)	Backgd.	Backgd. Count Rate x 10^{-3}	Max Count	Max Count Rate
1.010	X3YU0101M	NGC5139	512X512	1097.12	1.21	1.10	3373.63	3.07
1.020	X3YU0102M	NGC5139	512X512	1282.12	2.18	1.70	4881.63	3.81
1.025	X3YU0103M	INTFLAT	512X1024z	600.00	23.25	38.74	48.00	0.08
1.026	X3YU0104M	DARK	512X512	600.00	1.48	2.47	8.00	0.01
1.030	X3YU0105M	NGC5139	512X512	597.12	2.64	4.42	2198.00	3.68
1.040	X3YU0106N	NGC5139	512X512	2094.12	1.98	0.94	1223.00	0.58
1.045	X3YU0107N	INTFLAT	512X1024z	600.00	46.90	78.16	89.00	0.15
1.046	X3YU0108N	DARK	512X512	600.00	1.45	2.41	8.00	0.01
1.050	X3YU0109N	NGC5139	512X512	2877.12	2.24	0.78	157.00	0.05

Figure 5.7: Image and Orientation

Logsheet Line# 1.020 **Observation: X3YU0102M.C1H** **Proposal: 06930** *FOC*

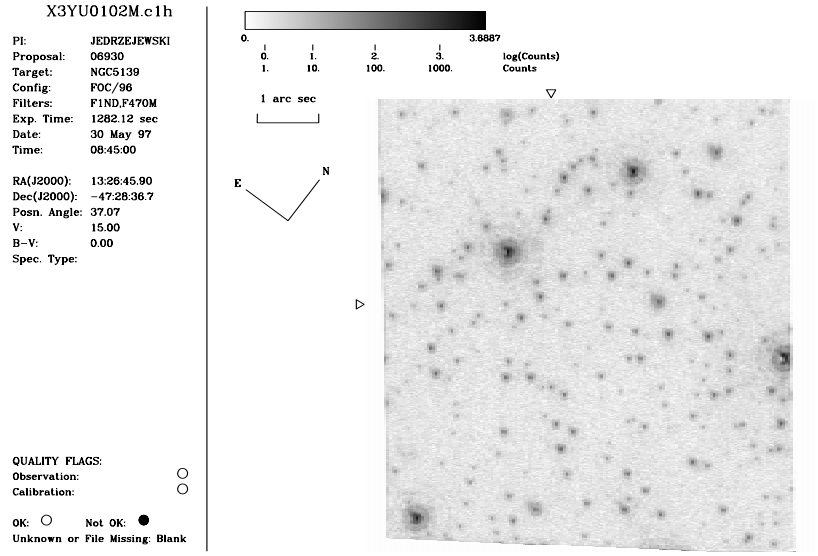

Figure 5.8: Performance and Exposure Summaries

Logsheet Line# 1.020 **Observation: X3YU0102M** **Proposal: 06930** *FOC*

HST Spacecraft Performance Summary

# Recenterings:	0	# Losses of Locks:	0
V2 Jitter (RMS):	3.0	V2 Jitter (PP):	72.1
V3 Jitter (RMS):	4.4	V3 Jitter (PP):	108.4

No apparent problems

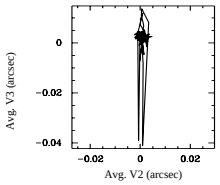

Exposure Summary

Target Name:	NGC5139
RA (J2000):	13:26:45.90
Dec (J2000):	-47:28:36.7
V:	15.00
B–V:	0.00
Spec. Type:	
Detector:	FOC/96
Filters:	F1ND,F470M
Aperture:	512X512
Exp Time (sec):	1282.1
Rootname:	X3YU0102M
Date:	30 May 97
Time:	08:45:00
Proposal:	06930
PI:	JEDRZEJEWSKI

Pipeline Processing and Calibration Data Quality Summary

The following throughput tables were used: crotacomp$hst_ota_005.tab, crfoccomp$foc_96_m1m2_001.tab, crfoccomp$foc_96_rflpri_002.tab, crfoccomp$foc_96_rflsec_002.tab, crfoccomp$foc_96_f1nd_002.tab, crfoccomp$foc_96_f470m_002.tab, crfoccomp$foc_96_rffocus_002.tab, crfoccomp$foc_96_n512_001.tab, crfoccomp$foc_96_dqe_004.tab

No Anomalies.

Calibration Status Summary

Switches and Flags

Keyword	Value	Calibration Step
BACCORR	OMIT	Background Subtraction
ITFCORR	OMIT	ITF Correction
PXLCORR	OMIT	Split Zoom Format Pixels
UNICORR	COMPLETE	Uniform DE Correction
WAVCORR	COMPLETE	Compute Photometric Par.
GEOCORR	COMPLETE	Geometric Correction
SDECORR	OMIT	Spectrograph DE Correction
		Blemish Correction

Reference Files and Tables

Keyword	filename	Pedigree
BACHFILE	xref$91b1313sx.r0h	
ITFFILE		
UNIHFILE	xref$f3716029x.r2h	INFLIGHT 1/11/1990 - 4/11/1990
GEOHFILE	xref$f371529ex.r5h	INFLIGHT 11/11/1994
SDEHFILE	N/A	
BLMHFILE	xref$d8i0905hx.r7h	

Chapter 6
FOC Calibration

In This Chapter...

This chapter describes the FOC calibration pipeline, discusses possible reasons for recalibrating your data, and shows you how to rerun the calibration tasks. It covers not only the calibration steps that are performed, but also the FOC image characteristics that are being calibrated and the derivations of those calibrations.

6.1 FOC Pipeline Processing

All data received by STScI from the Space Telescope Data Capture Facility pass through the Observation Support and Post-Observation Processing Unified System (OPUS)—referred to as the *pipeline*—to be processed and calibrated. The calibration software the pipeline uses is exactly the same as that provided within STSDAS under the **hst_calib** package (calibration software for Faint Object Camera is in the subpackage **stsdas.hst_calib.foc.focutility.calfoc**), enabling you to recalibrate any FOC data just as the routine calibration pipeline does. The calibration files and tables are taken from the Calibration Data Base (CDBS) at STScI and are usually the most up-to-date calibration files appropriate for the instrumental configuration used in the observation. (For additional details on the reference files used in the past, see also *FOC Instrument Science Report (ISR)* 082, available through the FOC pages on the World Wide Web).

The FOC calibration software (**calfoc**) takes as input one image: the raw `.d0h` file, and it produces two output images:

- A geometrically corrected image (`.c0h`).
- A geometrically corrected *and* flatfielded image (`.c1h`).

In addition, the calibration software takes as input any necessary calibration reference images or tables, and some engineering files. The calibration software determines which calibration steps to perform from the values of the calibration switches in the header of the raw data (.d0h) file (see also Table 6.1). Likewise, it selects the reference files to use in the calibration of the data by examining the reference file keywords. The appropriate values of the calibration switches and reference file keywords depend on the instrument configuration used, the date when the observations were taken, and any special pre-specified constraints. These parameters were set in the headers of the raw data file in the RSDP pipeline during the creation of the .d0h image.

6.2 FOC Calibration Switches

This section describes each of the FOC calibration steps, how they were determined, and how the pipeline task **calfoc** carries them out. Pipeline calibration of FOC imaging data:

- Dezooms zoom-mode images to produce square calibrated images.
- Determines the absolute sensitivity of the instrument configuration and sets photometry keywords allowing count rates to be converted to flux units.
- Corrects the geometric distortion of the image via interpolation of the data onto a rectified grid, creating a .c0h file.
- Applies a flatfield correction to the data that removes large-scale spatial non-uniformities, creating a .c1h file.

The flowchart in Figure 6.1 shows the steps of the **calfoc** pipeline process and the related calibration switches.

To determine the calibration steps applied to the data and the calibration reference files used to calibrate the data, look at the values of the calibration switches in the header of the raw (or calibrated) data. Before calibration, the calibration switches will have the value OMIT or PERFORM. The calibration process sets the switches for completed steps to COMPLETE in the header keywords of the calibrated data file.

6.2.1 Dezooming of Zoomed Images (PIXCORR)

A somewhat unfamiliar aspect to using the FOC is that the pixel size can be doubled in the *x* direction, with a corresponding increase in the field of view and a decrease in the horizontal resolution. This process is known as *zooming*. If an image has been taken in zoom mode, the first processing step is to invert this zooming process by splitting the data values along the first image axis (the sample direction). The length of the first axis (NAXIS1) is doubled, and the length of the second axis (NAXIS2) remains unchanged. If the zoomed image contained *n* rectangular pixels (50 x 25 microns each) in the sample direction, the dezoomed image contains 2*n* square pixels (25 x 25 microns), each with half the flux of the

Figure 6.1: Flowchart of the Calibration Process for FOC Data

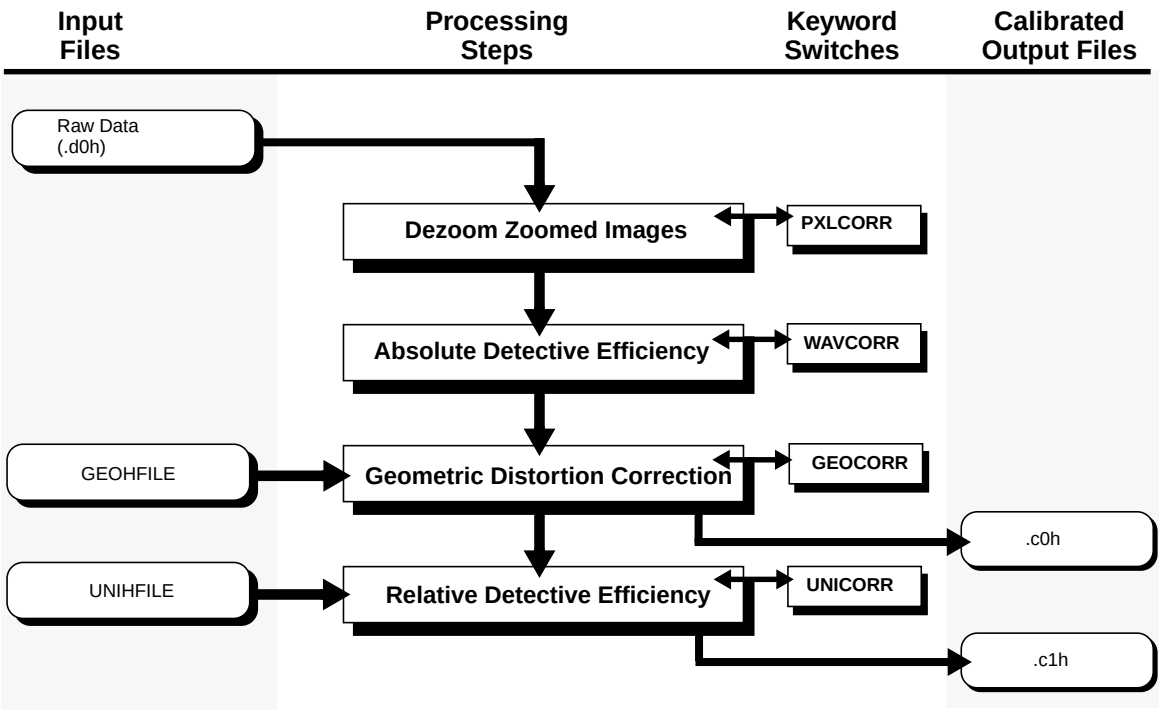

original rectangular pixel. No attempt is made to do anything more sophisticated. The keyword PXLCORR is set to COMPLETE when this step is done, and to OMIT when the image is taken using normal pixels.

6.2.2 Absolute Sensitivity Correction (WAVCORR)

This step does not modify the data itself, but instead computes a constant that can be used to convert the data values in the `.c1d` file to absolute fluxes. This constant is saved in the `.c1h` header file as the value of the PHOTFLAM keyword. The keywords that describe the absolute sensitivity (PHOTFLAM, PHOTMODE etc.) are derived using **synphot** (see page 3-16) applied to the photometric mode calculated using the instrument parameters. The photometric mode now includes the effect of format-dependent sensitivity (since May 18, 1994).

The sensitivity curve for the *f*/96 camera, often called the Detector Quantum Efficiency (DQE) curve, was derived from observations of a spectrophotometric standard through many of the medium and narrow band filters spanning the useful wavelength range of the detector. The DQE curve is combined with the filter transmission curves to derive the PHOTFLAM values or with **synphot** to convert measured counts into absolute flux values. The DQE derived for the *f*/96 relay is based on the flux that falls in a 1” radius aperture. This aperture size does not encompass all the flux from the star, especially in the UV. Note that this definition of the DQE treats all side diffracted or scattered light that falls outside the aperture as lost. If you wish to apply the DQE to different apertures or other photometric

Table 6.1: Calibration Switches in calfoc

Switch	Processing Step	Reference File
BACCORR	Remove instrument background by subtracting a dark count image; it is never done, for reasons given in the section titled "Background" on page 7-11.	bachfile
ITFCORR	Multiply by format-dependent inverse flatfield; it is never done, as will be explained in "Format-Dependent Effects" on page 7-9.	itfhfile
PXLCORR	Dezoom zoomed pixels by splitting each zoomed pixel in the sample direction into two pixels, each having half the flux of the original. Done only (but always) for data taken in zoom mode. Produces square pixels.	none
WAVCORR	Compute absolute sensitivity using throughput tables appropriate to observation mode (PHOTMODE). Names of actual throughout tables used are determined from graphtab and comptab tables. Names of throughput tables used are written to history section of calibrated data header. This step does not alter pixel values, it writes inverse sensitivity (PHOTFLAM), RMS bandwidth (PHOTBW), zero point magnitude (PHOTZPT), pivot wavelength (PHOTPLAM), and observation mode (PHOTMODE) to header of calibrated data.	graphtab and throughput tables
GEOCORR	Perform geometric correction to rectify optical and detector distortion using geometric correction reference file.	geohfile
UNICORR	Correct for large scale detector non-uniformity by multiplying by the uniform detector efficiency file, which is reciprocal of a highly-smoothed flatfield. Done only for images.	unitab, unihfile
SDECORR	Flatfield and compute absolute sensitivity for spectrographic data. At the moment, this step is not done.	sdecorr

methods, you should normalize your results to that aperture size using an appropriate PSF (see "Point Spread Function" on page 8-2).

The *f*/48 detector, for various reasons, has not been adequately calibrated in orbit. Only the pre-launch DQE curve has been used for the *f*/48 camera. On-orbit measurements taken in December 1993 showed that the measured fluxes from a spectrophotometric standard were about 60% of those expected. The *f*/48 curve was not updated with this information.

Multiplying the data values in the calibrated image by the value of PHOTFLAM and dividing the result by the actual exposure time (EXPTIME) converts the values to flux density F_λ in units of ergs cm^{-2} s^{-1} $Å^{-1}$. The current CDBS filter transmission, mirror reflectivities, and detector quantum efficiency curves are used to compute the conversion factor (PHOTFLAM) between detected count rate and a source flux F_λ averaged over the bandpass. The pivot wavelength, rms bandwidth, and zero-point magnitude are also saved in the header as the values of PHOTPLAM, PHOTBW, PHOTZPT, respectively. Finally, the observation mode (PHOTMODE) is written to the header, and this mode is used by **synphot** to determine the inverse sensitivity.

Status of Sensitivity Files

All COSTAR-corrected data taken before October 22, 1994, used the predicted DQE curve for the FOC+COSTAR sensitivity, with the measured DQE curve being applied to images taken after October 22, 1994. Therefore, the PHOTFLAM keyword will be incorrect for images taken prior to that date and should be recalculated if needed for data analysis. The actual files used to calculate these keywords are recorded in the HISTORY records at the bottom of the `.c0h` header file. The DQE file appropriate for COSTAR-corrected *f*/96 observations is `foc_96_dqe_004.tab`.

The DQE file appropriate for pre-COSTAR *f*/96 observations is `foc_96_dqe_003.tab`.

6.2.3 Geometric Correction (GEOCORR)

This correction removes both the *optical distortion* that arises in the telescope and the *detector distortion* produced by the electronic imaging system of the FOC. Optical distortion occurs upstream from the detector itself and arises primarily from the off-axis position of the FOC. Detector distortion occurs within the FOC's electronic imaging system, which consists of a three-stage image intensifier optically coupled to an Electron Bombarded Silicon (EBS) target TV tube.

Both the image intensifiers and the TV-camera section of the image system contribute to detector distortion. Intensifiers rely on an electric field for accelerating, and a magnetic field for focusing photoelectrons, and any irregularities in the uniformity of either results in distortion. The source of distortion within the target or TV camera section arises from the scanning of the target. This scanning distortion is due primarily to variations in the speed of the scanning beam at the ends of the sweep (where it must change direction), and the fact that the beam carries out an angular sweep across a plane target, with imperfections in the scanning electronics adding secondary effects. For these reasons, each video format has its own peculiar distortion characteristics, so the distortion measured for one format cannot be used directly to correct an exposure taken in a different format.

To facilitate correction of geometric distortion, reference points called *reseau marks* were etched onto the first of the bi-alkali photocathodes in the intensifier tube. These reseau marks form an orthogonal grid of 17 rows and 17 columns with a separation of 1.5 mm (60 pixels), each reseau being 75 microns (3 x 3 pixels) square. The detector distortion was originally determined by illuminating the photocathode with an internal light source, i.e., an internal flatfield. The observed positions of the reseau marks, when compared to the expected positions, provided a map of the detector distortion across the field. The optical component of the distortion was determined independently from ray-tracing models of the HST and FOC optics and was applied to the reference reseau grid to give the expected positions.

Unfortunately, the detector distortion for the FOC clearly showed variations on spatial scales smaller than the spacing of these reseau marks, particularly near the scan line beginning, and therefore models based only on the reseau marks inadequately represent the true distortion. A new method of determining distortion based on overlapping observations of crowded starfields was developed to determine the net distortion (the optical distortion is naturally folded into this new method). These observations yielded a two-dimensional spline distortion model from which the new geometric correction files were generated. The new scheme removes distortion by transforming each pixel in an undistorted image to a quadrilateral virtual pixel in the distorted image using the derived distortion model. The flux within the distorted pixel is then calculated as the sum of the contributions from each pixel the distorted pixel covers, where the weightings are simply the areas common to distorted and undistorted pixels. This procedure is illustrated in Figure 6.2. Because the transformed pixels fit together with no gaps and cover the distorted image completely, the method is rigorously flux-conserving. The improvement in quality is most apparent for smaller formats where the small number of visible reseau marks prevented the determination of a good model.

Figure 6.2: Pixel Transformation

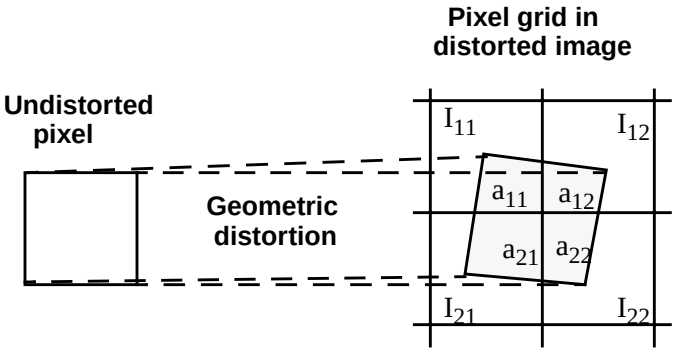

$$I_{resampled} = I_{11}a_{11} + I_{12}a_{12} + I_{21}a_{21} + I_{22}a_{22}$$

If you need the finest possible spatial resolution, bear in mind that this method applies a position-dependent smoothing to the data. You might find working with the raw uncorrected data more profitable if you need to preserve every detail.

The keywords PXFORMT, SAMPPLN, LINEPFM, SAMPOFF, and LINEOFF indicate the format in which the image was taken and therefore determine the appropriate geometric correction file. Geometric correction files exist for most formats listed in Table 4.2 and Table 4.3. The keyword GEOCORR tracks the execution of this step and is set to COMPLETE upon creating the `.c0h` file. In addition, the keyword GEOHFILE lists the geometric correction file that was applied to the image, which can be useful in making sure that the proper correction was applied.

Status of GEOHFILE

The new geometric correction files have been used in the calibration pipeline for *f*/96 data since March 19, 1995 (*f*/48 geometric correction files are still based on reseau marks). Only observers who want sub-pixel accuracy in position measurements or those who have used the 256 x 256 format should even consider reprocessing their old data with the new geometric correction files. For most observers, the improvements will not significantly affect positions or photometry.

6.2.4 Flatfield Correction (UNICORR)

This correction is referred to as the uniform detective efficiency (UNI) correction. It attempts to remove the effects of non-uniform efficiency of the detector, and its complicated name is really just another way of saying "flatfielding." The procedure first selects the appropriate correction file on the basis of wavelength. The pivot wavelength of the bandpass (OTA + filters + detector) is used to select the correction file with the closest wavelength (in the geometric sense). The UNI correction files are 1024 x 1024 images from which the appropriate sub-image is extracted to match the image format of the science image. For example, a science image taken in the standard centered 512 x 512 format will use the center 512 x 512 of the appropriate UNI correction file whereas a 512 zoomed x 1024 format science image will use the whole UNI correction file (recall that the science image has been dezoomed in the pipeline process). These files are heavily smoothed to correct large-scale features extending more than 20 pixels and are geometrically corrected with the current geometric correction file. The calibration is then performed by multiplying the science image by the UNI sub-image given by the keyword UNIHFILE. The UNICORR keyword is then set to COMPLETE when this step is finished, and OMIT if it is not executed.

Status of UNIHFILE

The current UNI files are derived from the same observations that produced the pre-COSTAR corrections; external observations taken at 1360Å, and internal flatfields at 4800Å, 5600Å, and 6600Å. The difference between the pre-COSTAR and post-COSTAR UNI files lies in the geometric correction. The installation of COSTAR changed the optical distortion of the *f*/96 field, which is rectified in the geometric correction step. The latest UNI files, for COSTAR-corrected *f*/96 observations, are the pre-COSTAR UNI files corrected with the post-COSTAR geometric correction file.

The pre-COSTAR UNI files are derived from pre-COSTAR observations taken at 1360Å, 4800Å, 5600Å, and 6600Å, to which we have applied the pre-COSTAR geometric correction file.

6.3 Reasons to Recalibrate

FOC data files retrieved from the Archive were calibrated with the best calibration reference files available at the time the data were taken. You can use StarView, as described in Chapter 1, to determine both the reference files used in the original observation and the reference files now considered the best for calibrating that observation. (See *FOC ISR* 082 for a complete listing of calibration reference files.). However, discrepancies between these lists do not always mean that it is necessary to recalibrate, because the effect on the data might be merely to redistribute the noise slightly rather than to add anything significant to the signal. It is worth emphasizing that *there are very few situations where recalibration will significantly improve FOC science data.* FOC calibration files do not change frequently, and the changes that do occur tend to be minor.

The five reasons why a user might want to recalibrate FOC data relate to:

- New sensitivity information for the OTA+COSTAR+FOC system (e.g., new format-dependent sensitivity ratios, re-calibration of the FOC DQE curve).
- New flatfield reference files.
- New geometric correction reference files.
- Redesigned pipeline or introduction of new calibration modes.
- User-derived calibrations.

6.3.1 Absolute Sensitivity Keywords

You can account for changes in sensitivity information without recalibrating the data. Instead you can run tasks in the **synphot** package using the PHOTMODE relevant to the data. For example, suppose you want to redetermine the absolute sensitivity of exposure `x28t0203t`, a 256 x 256 *f*/96 image taken in February 1994, shortly after COSTAR was inserted. At that time, the COSTAR keyword was not correctly inserted into the PHOTMODE string, nor was the format-dependent sensitivity correctly recorded. The PHOTMODE for this particular observation is “FOC F/96 F2ND F1ND F346M”, whereas it should read “FOC F/96 COSTAR F2ND F1ND F346M X96N256”. Also, the HISTORY records show that the pre-COSTAR DQE file was used (`foc_96_dqe_003.tab`) rather than the in-flight calibrated `foc_96_dqe_004.tab`. The resulting inverse sensitivity in the header was

```
PHOTFLAM =          7.635416E-17 / Inverse Sensitivity
```

Recalculating using the **bandpar** task in the **synphot** package with the correct PHOTMODE and the most recent DQE file gives:

```
PHOTFLAM =          7.811949E-17
```

(Note that the URESP parameter that **bandpar** calculates is identical to PHOTFLAM.) The difference is not large, but it consists of a 25% increase, due to the inclusion of the format dependent sensitivity for the 256 x 256 format, and a 23%

decrease, due to the inclusion of the COSTAR mirror reflectivities. The effect of the updated DQE curve is negligible at that wavelength.

Recalibrating the absolute sensitivity keywords is slightly more tricky for pre-COSTAR data, because you must then tell **synphot** that COSTAR is not in the beam and to use the pre-COSTAR absolute sensitivity file. The first item is simple to deal with: just insert the value “nocostar” in the PHOTMODE string, e.g.:

```
band(foc,f/96,nocostar,f486n,x96n256)
```

The second item is more difficult to address: you must edit the HST component table available through the calibration reference file screens in StarView (see “Identifying Calibration Reference Files” on page 1-19). The most straightforward way to proceed is to **tcopy** the component table to a local working directory, **tedit** the file so that the COMPNAME `foc_96_dqe` (on line 605 or so) has the FILENAME `crfoccomp$foc_96_dqe_003.tab`, and then write the edited file to a new version with a different name. Then the task **refdata** can be used to make a parameter file that has a component table that refers to the pre-COSTAR FOC sensitivity file. Subsequently, **calcphot** can be run with **refdata** pointing to that new parameter file.

6.3.2 Flatfields

When new flatfields based on new flatfield data are delivered, it might be profitable to recalibrate by reapplying the flatfield. However, the only new flatfield deliveries were those derived in the ultraviolet using the Orion nebula as a target and those constructed in 1990 using internal flatfields taken during the Science Verification phase immediately after the launch of HST. The new flats from March 1995 were basically the same as the old flats except geometrically corrected using the new geometric correction files.

6.3.3 Geometric Correction Files

Delivery of new geometric correction files often lures users into thinking that they need to recalibrate their data using the most up-to-date reference files. In fact, this correction is rarely necessary, because the main effect is in improving the astrometric accuracy of the data. The photometric quality barely changes, because the geometric correction algorithm rigorously conserves flux, so the new correction merely redistributes the noise. Users who need the utmost astrometric accuracy (e.g., for proper-motion studies) will want to take advantage of improved geometric calibration files. However, they will still be left with some time-dependent positional uncertainty (see page 7-9) unless they take their own internal flatfields and calibrate out the time dependence of the geometric distortion themselves.

6.3.4 Improved Pipeline Algorithms

The fourth item is a catch-all for those situations where STScI staff are able to improve on the pipeline correction algorithm. Such a situation occurred in November 1991, when the order of processing changed so that geometric correction is performed before flatfielding. A more thorough discussion of this change and the rationale behind it is described in *FOC ISR* 051. Note that all FOC files in the Archive reflect this change because the entire Archive has been reprocessed in the meantime.

6.3.5 User Calibrations

The last item is for those users who have decided that the pipeline calibration is not sufficient for their needs or has compromised the quality of the data. For example, 8-bit overflows in 512 x 1024 data can often be corrected by adding integral multiples of 256 to the pixel values in the `.d0h` file until the intensity distribution is correct. You cannot repair the pipeline-corrected data in this way because the geometric correction algorithm smooths the overflowed pixels and mixes them with their neighbors. In that case, you must repair the `.d0h` file first and then recalibrate.

Alternatively, you might need to flatfield using an unsmoothed flatfield. In that case, the images must be lined up very accurately so that features on the photocathode (reseau marks, blemishes etc.—see pages 4-7 through 4-10) divide out properly. Extreme care is required in order to avoid misalignment artifacts.

6.4 How to Recalibrate

Once you have determined that recalibration is necessary, you can either rerun **calfoc** using the correct reference files or rerun the individual STSDAS tasks that perform the desired operations. Before recalibrating, make sure you obtain the desired reference files. The easiest way to obtain calibration reference files is via StarView, as described on page 1-19.

To recalibrate using **calfoc**, first assemble your set of calibration reference files. You can then use the task **chcalpar** in the **stsdas.hst_calib.ctools** package to edit the header parameters in your `.d0h` file so that they point to the desired calibration files. After you have set these parameters, run the **calfoc** task, and it will produce recalibrated FOC data files.

If you would rather execute the individual steps using the appropriate IRAF tasks, these are the steps to apply:

- ***Dezooming***: Use **stsdas.hst_calib.foc.focphot.dezoomx**. This step is straightforward.
- ***Absolute sensitivity keywords***: Use **stsdas.hst_calib.synphot.bandpar** as described in “Absolute Sensitivity Keywords” on page 6-8 or **stsdas.hst_calib.synphot.calcphot** as described on page 3-16.

- ***Geometric correction***: Use **stsdas.hst_calib.foc.focgeom.newgeom**. Again, this step is relatively straightforward.
- ***Flatfielding***: Use **iraf.images.imarith**. Remember to use the appropriate subset of the full-format flatfield and to *multiply* the data by the reference file, unless of course the flatfield has been derived by the user and is not inverted. For a 512 x 512 normal format image the appropriate IRAF command might be:

```
fo> imarith image.c0h * flatfield.hhh[257:768,257:768] \
>>>  image.c1h
```

Chapter 7
FOC Error Sources

In This Chapter...

The pipeline processing described in the previous chapter attempts to remove most of the instrumental signatures of the FOC detector. Pipeline processing does not remove all of the instrumental features because some of the FOC's properties are either time dependent, varying in a random way that precludes correction, or else difficult to correct without introducing other errors. This section highlights some limitations of the pipeline calibration and certain other effects that the pipeline does not address.

7.1 Overview of FOC Characteristics

Table 7.1 lists certain effects owing to the design of the FOC detector, optics, and electronics that afflict all FOC images and indicates whether the pipeline corrects for them. .

The diagram below (Figure 7.1) describes where these various instrumental characteristics arise.

Table 7.1: Characteristics Corrected in Standard Pipeline

Characteristic	Pipeline Corrected?
Nonlinearity and saturation	No
Geometric distortion	Yes
Flatfield residuals (i.e., blemishes, reseau marks, defects, and video effects)	No
Format-dependent sensitivity	Yes
Background noise	No
Filter-induced image shifts	No
Point spread function	No

Figure 7.1: Sources of Instrumental Characteristics

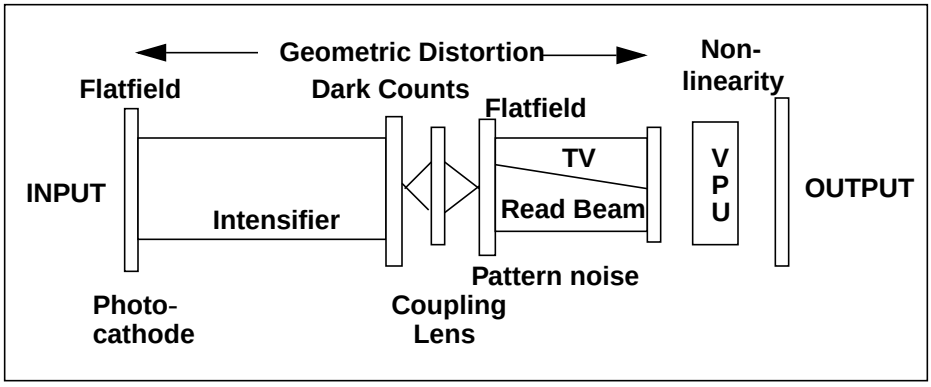

The ideal calibration algorithm applies to the raw data the inverse transformation to that which converted the input image to the output image. Each step would apply the corrections in reverse order, starting with the nonlinearity correction. In practice, the individual components of the ideal transformation are not known accurately, so such a process is unrealistic. Therefore, some of these effects are addressed only partially in the pipeline while others are not corrected at all. The following sections describe the limitations of these calibrations and their effects on the uncorrected image characteristics.

7.2 Nonlinearity

At high count rates, the video processing unit (VPU) of the FOC *undercounts* photon events, resulting in a nonlinear count rate. At even higher count rates, the detector saturates. An image whose counts have saturated will develop a dark hole, with a bright crescent appearing to one side (see Figure 4.6). The FOC remains linear to much higher count rates for point sources than for uniform

sources.[1] Table 7.2 gives the nonlinearity and saturation thresholds separately for extended and point sources and the different formats and modes of the FOC. Here, a uniform source is defined to be one in which the flux varies by less than +/– 10% on scales of 10 pixels, and the nonlinearity threshold is defined to be the count rate at which the FOC exhibits nonlinearity at the 10% level.

Table 7.2: Nonlinearity Parameters for Extended Sources and Point Sources

		Uniform Source		Point Source (for peak count rate)	
Camera	**Format**	**N (nonlinear)**	**N (saturation)**	**N (nonlinear)**	**N (saturation)**
f/96	512 zoom x 1024	0.04	0.11	0.15	0.45
	512 x 1024	0.08	0.37	0.5	1.5
	512 x 512	0.15	0.73	1.0	3.0
	256 x 256	0.60	2.93	4.0	12.0
	128 x 128	2.40	11.7	16.0	48.0
f/48	512 zoom x 1024	0.03	0.07	0.09	0.27
	512 x 1024	0.05	0.26	0.35	1.05
	512 x 512	0.06	0.52	0.70	2.10
	256 x 256	0.40	2.09	2.80	8.40
	128 x 128	2.40	8.40	11.3	33.9
f/48 SPEC	256 zoom x 1024	0.03	0.13	0.18	0.53
	256 x 1024	0.10	0.52	0.70	2.1

If the count rate from a point-like target is in the nonlinear regime, you should take special precautions when determining its brightness. For example, you might consider measuring the flux in the wings of the PSF and scaling them to a linearly exposed PSF. Unfortunately, no reliable and robust method exists for correcting nonlinearity in the FOC. There are, however, a couple of useful approaches for correcting some of the nonlinearity in calibrated FOC images, depending on whether the intensity distribution uniform or point-like.

Nonlinearity is introduced at the last stage of the FOC imaging process, so you should apply any nonlinearity corrections before geometrically correcting and flatfielding the image. The correction to apply to a given pixel depends on both the count rate in the pixel and the rates in neighboring pixels. If the count rate remains relatively constant over scales of 10–20 pixels or so, then the nonlinearity will be more severe than for a single pixel with the same count rate surrounded by pixels with a lower rate, such as in the center of a stellar PSF.

1. A typical photon event is several pixels by several pixels in size, and for extended (or *uniform*) sources the photon events at a given pixel affect those at the neighboring pixels.

This procedure was extended by Greenfield in *FOC ISR* 074. He hypothesized that the actual flux distribution within a given aperture was not as important as the mean count rate. By looking at pre-launch test FOC images he was able to determine that convolving images of PSFs with a circular aperture with radius 5.5 pixels yielded a nonlinearity correction very similar to what a flatfield would give. A more detailed discussion of this procedure is beyond the scope of this manual, but readers are referred to *FOC ISRs* 074 and 073 for some suggestions on how to deal with nonlinearity for stellar fields.

If the count rate for a *uniform* source is in the nonlinear regime, but below the saturation value, it is possible to correct the pixel values for nonlinearity using the **fflincorr** task in the STSDAS **foc.focphot** package. The **fflincorr** task uses the FOC linearity curve which has been derived for uniform sources from internal lamp flatfields. The linearity curve follows the formula $\rho = a(1 - e^{(-r/a)})$, where ρ is the observed count rate, *a* is the uniform source saturation count rate as given in Table 7.2, and *r* is the *true* count rate. This correction can be applied only for small or moderate nonlinearity; it is not valid for high nonlinearity. Users should beware that these methods are somewhat preliminary, and they are not guaranteed to correct (or even improve) all types of data. Do not apply this correction blindly.

7.3 Geometric Correction

The current geometric correction algorithm is good at correcting the gross characteristics of the FOC's geometric distortion, rectifying it to 0.5 pixels rms over most of the imaging format. However, the plate scales and orientations of FOC images are known to be time-dependent. The maximum change in scale from just after switch-on until the FOC has stabilized fully was measured during the initial orbital verification to be approximately 0.3%. A systematic study of the time dependence of the plate scale has not been done since, but repeated observations in the crowded-field analysis of fine-scale distortions (see page 6-6) did show plate scale differences of 0.1–0.2% even after the FOC had been warmed up for a long time. Angular rotations on the order of 0.1% from exposure to exposure can also occur. The pipeline does not attempt to correct for time-dependent aspects of the geometric distortion, and this deficiency can lead to astrometric errors between images taken at different times.

Geometrically corrected images displayed with high contrast close to the background, often show relatively low-frequency *fringes* with scale lengths of between 40 and 100 pixels (see Figure 4.5). This effect, a product of the geometric correction procedure caused by the algorithms used in re-binning the data, is merely a modulation of the noise characteristics of the data. The mean intensities in the image are not affected.

7.4 Flatfield Residuals

There are currently four UNI (flatfield) files for the *f*/96 camera at 1360, 4800, 5600, and 6600 Å and two UNI files for the *f*/48 camera at 3345 and 4800 Å. The UNI files have been derived from heavily smoothed flatfields. Thus, they do not flatten small-scale features, such as scratches and reseau marks, that exist in the flatfield response and can affect your photometric accuracy.

How much the small scale features affect the accuracy depends greatly on the type of data and the method of analysis. In some cases, careful treatment can improve the calibration. Figures 7.2 and 7.3 show relatively high signal-to-noise full-format flatfields obtained in the UV for the *f*/96 and *f*/48 cameras, respectively. Many of the features to be discussed here are evident in those figures.

7.4.1 Border Effects

The borders of FOC images suffer from corruptions arising both inside and outside the detectors. Among the most obvious external effects are the finger-like shadows cast by the occulting fingers (two occulting fingers for *f*/96 and the slit location finger for *f*/48.) In addition, square masks in front of both detectors shadow the upper left and lower left corners of the *f*/96 image (upper and lower left) as well as the lower right corner of the *f*/48 image. Furthermore, geometric correction transforms the straight edges of the original raw images into curved edges, most noticeable on the left and right sides.

Internal border effects show up in a few bad rows at the top and bottom of the raw image and the left-most columns of the raw image as well as a significant number of columns at the beginning of the scan line (right side of the image). In all FOC images, the internal border effects are present regardless of format; however, they do change from one format to another. In particular, the corrupted pixels at the beginning of the scan line arise from defects in the beginning of the sawtooth in the scanning waveform. The corrupted beginning is about 5% of the scan line for most *f*/96 formats In the *f*/48 detector it gets progressively worse for smaller formats (from about 5% for the full format to about 25% for the 128 x 128 format). The horizontal stripes seen in the bottom left of the *f*/96 image result from a ripple instability of the coil drivers at the beginning of a frame scan. None of these effects are normally correctable.

Figure 7.2: f/96 External UV Flatfield Image

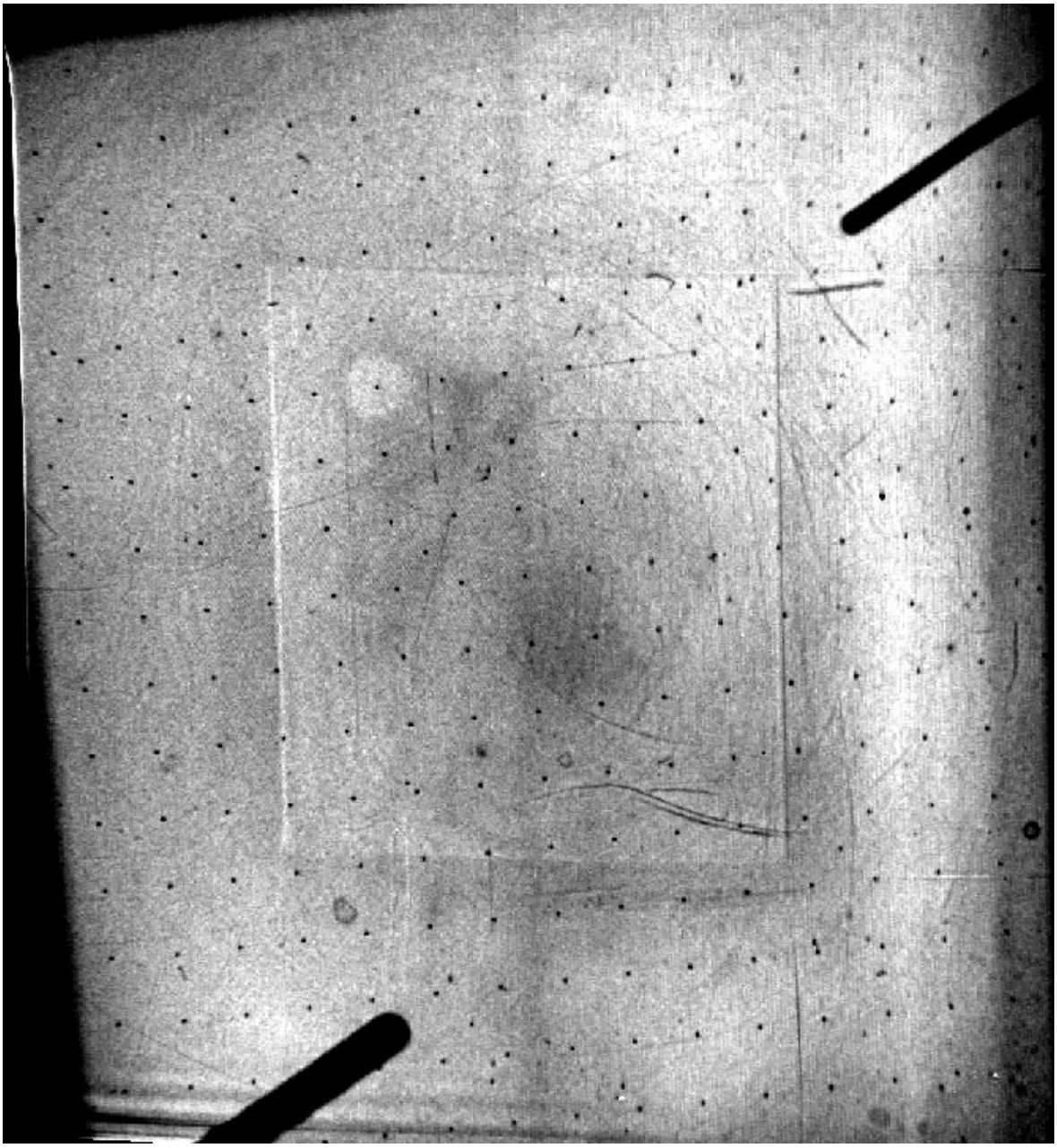

Figure 7.3: f/48 External UV Flatfield Image

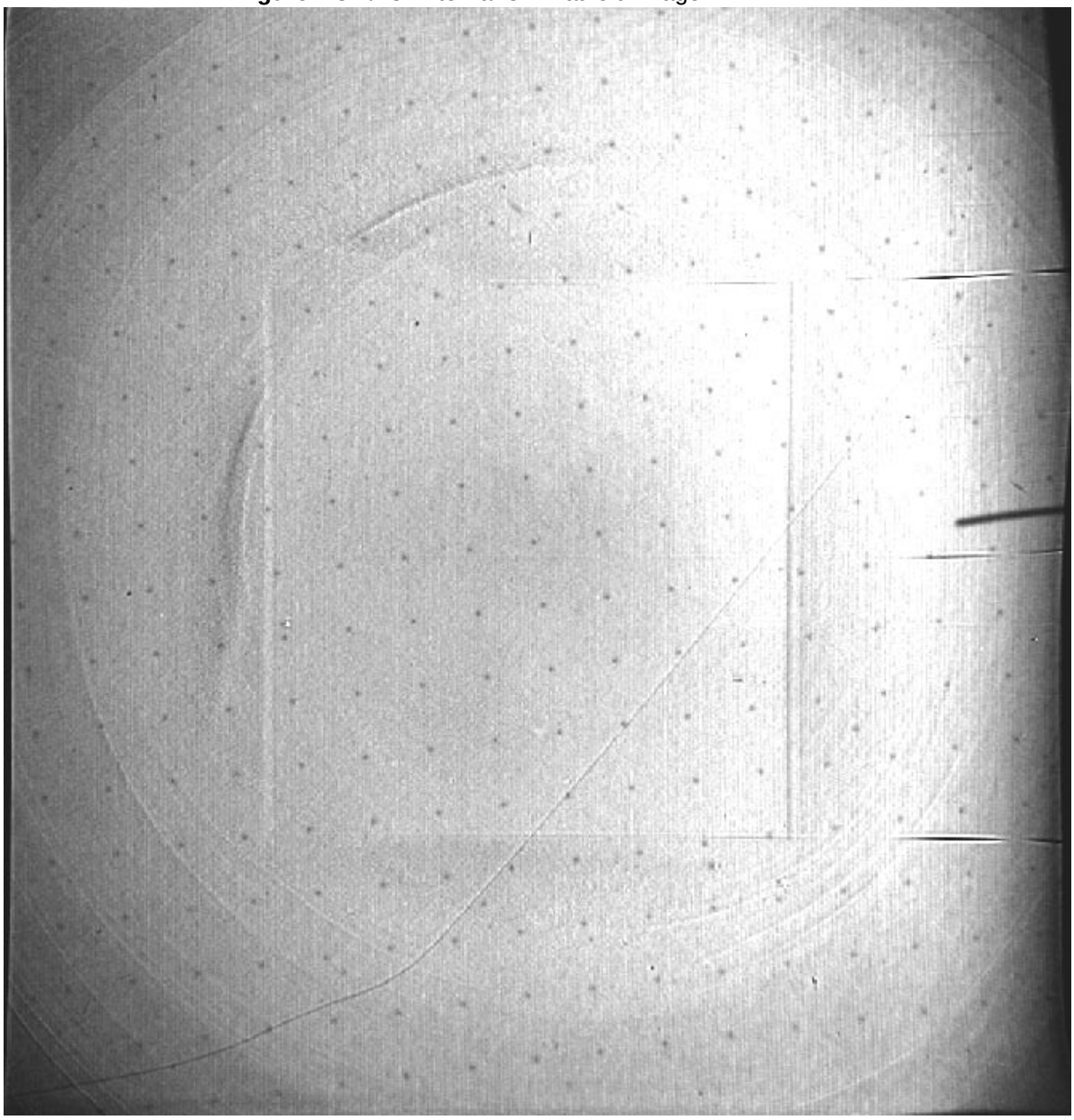

7.4.2 Video and Digitizing Defects

The narrow line running from the bottom left corner to the upper right corner (clearly visible for *f*/48, less so for *f*/96) is due to the read beam of the television camera not being completely blanked before it flies back to the beginning line at the end of a frame scan. This effect, along with a change in path, becomes more noticeable in smaller formats. The narrow horizontal features at the right edge, especially at lines 256, 512, and 768, are due to noise glitches on the scan coil driver caused by changes in the most significant bits of the line counter. The central 512 x 512 pixels in both cameras are outlined by sharp changes in

sensitivity. Heavy use of the 512 x 512 format has burned a charge discontinuity into the camera target array at the edges of this format. None of these effects is normally correctable and the affected areas should be treated as bad pixels.

7.4.3 Reseau Marks, Scratches, and Blemishes

A regular grid of reseau marks used to measure detector distortion spans both detectors' photocathodes. These reseau marks have about 90% opacity and are not normally worth trying to flatfield. In addition to the reseau marks, there are various scratches and blemishes, much more numerous in the *f*/96 camera. The scratches and blemishes generally appear much deeper in the far-UV—as much as 30% opacity for some scratches. Because the pipeline flatfield correction is heavily smoothed, none of these effects will be flatfielded out. Hence, photometry of sources which fall on or near these image defects can be compromised.

The **imedit** task in the **images** package or the **rremovex** task in **focphot** package can be used to repair such cosmetic defects in images having a source that falls on a reseau mark or small scale blemish. These tasks replace the values of the affected pixels with the average values of their neighboring pixels. Great care, however, must be taken in interpreting photometric results for sources which are directly affected by such image defects (i.e., in which the peak of the source falls on or immediately adjacent to an image defect).

7.4.4 Pattern Noise

Pattern noise, neither fixed nor constant in magnitude, constitutes another source of non-uniformity. Two types of patterns are often present, although not always easily seen in low count extended areas or flatfields. The more noticeable one is an approximately sinusoidal pattern with its peaks and troughs oriented at an approximately 45 degree angle and a period of 3.35 pixels for *f*/96 (it is just barely discernible in Figure 7.2). It is believed to originate from a moiré effect between a TV tube grid and the diode array on the target. The amplitude of the pattern depends on the count rate in the area. In flatfields with count rates between about 0.02 and 0.1 counts pixel^{-1} s^{-1} for a 512 x 512 format, the rms amplitude of the pattern is about 5% of the flatfield counts for *f*/96 and about 2.5% for *f*/48 (the peak deviations from a flat response due to this pattern are at least twice these values). At lower count rates, threshold unknown at this time, the pattern disappears. On the other hand, the pattern intensifies when count rates are in the nonlinear regime and thus is much more easily seen. In fact, it is a quick way of recognizing serious nonlinearity in an image.

A second pattern arises from some form of interference with an FOC digital timing waveform that has a four-pixel period. It shows up as vertically striped patterns on the flatfields (visible in Figure 7.2). Although very coherent in orientation and frequency (in the raw image), the details of the modulation do not appear to remain constant in either phase, waveshape, or amplitude from image to image. The rms amplitude of this pattern in moderate count-rate flatfields, is

approximately 2.5% for both cameras. Like the 45 degree pattern, this pattern seems to disappear at low count rates.

Given the nonlinear nature of the amplitude of these patterns and their variability in position (phase), there is no general method for correcting them. When count rates are moderate across most of the image, i.e., from an extended object or PSF halos, Fourier techniques can sometimes proves useful in removing the pattern. The main purpose of these techniques should be viewed as providing aesthetically pleasing images rather than as improving photometric accuracy.

7.4.5 Large Scale Variations

Large scale variations are those spatial variations having relatively low spatial frequencies, i.e., 20 or more pixels. The UNICORR step in the pipeline attempts to remove such variations from the image. Large scale variations in the response of the FOC do not appear to depend strongly on wavelength between 1300 and 6000 Å; generally speaking, the large scale response does not change more than 10% for all pixels except at the edges and corner of the full format. Beyond 6000 Å, the flatfields begin to change significantly, generally with poorer relative sensitivity towards the corners.

Obtaining flatfields in the UV requires a great deal of spacecraft time for each wavelength desired. At the moment, only one UV flatfield each exists for the *f*/96 and *f*/48 camera (at 1360 and 3727 Å respectively). It is not likely that there will be any more UV flatfields obtained for *f*/48.

The *f*/96 large scale response appears to be accurate to 1 to 2% rms over the most of the photocathode at the wavelength where it was obtained, excluding the edges and corners, and regions where the scanning oscillations are significant. The accuracy for *f*/48 is estimated to be 2 to 4% rms over comparable areas.

7.4.6 Time Variability

A small amount of temporal variability has been observed in the flatfield response; it is largest just after the FOC is turned on and begins taking exposures. Changes of about 1 to 2% are seen with respect to the flatfield response after an hour of exposures. The changes for *f*/48 are about twice as large. In general the response at turn on is higher at the center and weaker at the edges of the full format.

7.4.7 Format-Dependent Effects

The FOC flatfield depends on the video format used (Greenfield and Giaretta, 1987, *FOC ISR* 024). You cannot just divide an image by a flatfield derived from the corresponding subsection of the full-format field, even if you take great care to align the two images so that the reseau marks overlap. This effect was suspected to be due in part to the limited resolution of the geometric distortion field provided by the reseau marks and the resulting change in the apparent pixel size with

position. More detailed analysis by Greenfield using the new geometric correction method described on page 6-5 showed that these suspicions were ungrounded. The variations in sensitivity with position truly depend on the video format. At this time, however, the appropriate correction files have not been derived, although the possibility of applying a format-dependent flatfield does exist within the current FOC pipeline.

7.5 Format-Dependent Sensitivity

The sensitivity of the FOC depends on the format being used. The overall (OTA + COSTAR + FOC) central absolute quantum efficiency $Q(\lambda)$ in counts photon^{-1} (DQE), plotted in Figure 4.3 and tabulated as a function of wavelength in Table 11 of the *FOC Instrument Handbook* (version 7.0), refers to the 512 x 512 format. Because the DQE is a function of detector format whose cause is unknown (see *FOC ISR* 075), we give in Table 7.3 the sensitivities of the other formats, relative to the 512 x 512 format. Typical uncertainties in these numbers are approximately 5%.

Table 7.3: Format-Dependent Sensitivity Ratios

Camera	Format (FxL)	Relative Sensitivity
f/96	512*z* x 1024	1.25
	512z x 512	1.45
	512 x 512	1.00
	256x256	1.20
	128x128	1.23
f/48	512*z*x1024	1.44
	256*z*x1024	1.28
	512x1024	1.02
	512x512	1.00
	256x256	0.85

The pre-COSTAR overall (OTA + FOC) central absolute quantum efficiency Q(λ) in counts photon^{-1} (DQE) with no filters in the beam is plotted and tabulated as a function of wavelength in Figure 28 and Table 12 of the *FOC Instrument Handbook,* version 3.0, for the FOC imaging and spectrographic configurations. The data represent the product of in-orbit measurements for the *f*/96 camera and ground-based measurements of the *f*/48 absolute quantum efficiency, reflectance measurements of the OTA primary and secondary mirrors witness samples and an arbitrary dust covering factor of 10%. Pre-COSTAR data are not automatically corrected for format-dependent sensitivity effects.

7.6 Background

The FOC suffers from various types of background, the most important of which are thermal electrons, Cerenkov radiation from high energy particles, geocoronal emission lines, zodiacal light, and light scattered within HST from the bright Earth or Moon. Because the particle-induced background levels are essentially unpredictable, the FOC pipeline does not attempt to remove the background from a geometrically corrected and flatfielded image. In practice, most astronomical data analysis procedures derive the background locally as needed, so pipeline background removal is unnecessary.

The levels, spatial distribution, and time variation of the principal sources of background are discussed below to help you decide whether the background on your images might be astronomically interesting or is merely an instrumental effect. For a more thorough discussion, see the *FOC Instrument Handbook*.

7.6.1 Detector Background

The detector background arises primarily from thermal electrons at the first photocathode and high energy particles. The dark current due to thermal electrons is rather lower than the particle-induced background, at approximately 2×10^{-4} counts/sec/pixel. This background source is likely uniform over the field and temporally stable and does not show the reseau marks as dark holes. The particle-induced background is caused by high-energy electrons and protons which generate intense flashes of Cerenkov radiation as they pass through the photocathode window. The FOC's video processing unit (VPU) cannot distinguish the photons from these flashes from celestial photons, and so they appear as a background. The flux of these particles rises strongly over the South Atlantic Anomaly (SAA), but even well away from the SAA, they are the principal contributor to the background of most FOC images. For most of the useful orbit of HST, the particle-induced background is of the order of 7×10^{-4} counts sec^{-1} pixel^{-1} on the *f*/96 side, and $1\text{-}3 \times 10^{-3}$ on the *f*/48 channel. Upward fluctuations of these values are sometimes recorded. Because the particle-induced background generates photons, its spatial distribution looks like a flatfield, except

the shadows at the edges of the field caused by obstructions in the FOC beam between the aperture plate and the photocathode are not present. The reseau marks are between the photocathode faceplate where the Cerenkov radiation originates and the photocathode, so they will show up in exposures dominated by such backgrounds.

7.6.2 Geocoronal Emission Lines

The most important contributors to the background at ultraviolet wavelengths are geocoronal emission from Lyman-α (1216 Å) and the O I triplet at 1304 Å, which are relevant only during daytime observations. From on-orbit measurements using the *f*/96 camera, the former background has been found to vary with solar zenith distance (ZD); see Sections 6.4, 6.5, and 7.0 of the *FOC Instrument Handbook*, version 7.0, for more details. When the zenith angle is less than 160 degrees, the Lyman-α emission is zero.

For O I 1304, the background is less than 5×10^{-5} counts/sec/pixel for solar zenith distances (ZDs) of more than 90 degrees, rising nonlinearly to about 8×10^{-4} counts sec^{-1} $pixel^{-1}$ at ZD of 25 degrees.

For *f*/48, these numbers should be multiplied by a factor of about four, reflecting the pixel-size difference.

7.6.3 Zodiacal Light and Diffuse Galactic Background

The contributions to the FOC background from zodiacal light and diffuse galactic background have not been measured with the telescope in orbit, so you should assume that the information in the *FOC Instrument Handbook*, version 7.0, is the best available. Typically, the particle-induced background dominates in an *f*/96 image under all but the most extreme conditions (e.g., on the ecliptic and pointing as close to the sun as constraints allow), when the zodiacal background and detector background become comparable. Similarly, the diffuse galactic background can be ignored for almost all situations.

7.6.4 Scattered Stray Light

Normally, the FOC background is dominated by the detector, by zodiacal light in the visible, and by geocoronal Lyman-alpha and diffuse galactic light in the far UV. However, stray light reaching the OTA focal plane due to scattering from the baffle system, the OTA tube, and dust on the mirror can dominate the background when a bright object such as the sun, moon, or the bright Earth limb is nearby. In-orbit calibrations of this stray light have been performed by P. Bely and D. Elkins using a solar spectrum combined with the Earth's and the moon's albedo. Only for observations where the limb angle is less than 50 degrees from either the moon or the Earth will stray light have an illumination brighter than 23 V magnitudes per $arcsec^2$ at wavelengths greater than 3400 Å. More details on the

determination of the stray light contribution and its wavelength dependence can be found in Section 6.5 of the *FOC Instrument Handbook*, version 7.0.

7.7 Filter Induced Image Shifts

The FOC filter wheels hold the filters roughly parallel with the photocathode of the FOC, but slight offsets can shift the image position. The offset of the F320W filter, an image shift of 80 pixels, means a centered target is thrown about 80 pixels towards the edge of the image when the F320W filter is put in place.

Most FOC filters in the visible band induce an image shift of over 7 pixels, or over 0.1”, in an *f*/96 image. These effects can confuse the identification of an object imaged through different filters if the appropriate filter shifts are not taken into account. They can also make it difficult to obtain the proper offset for a dispersed prism image. Table 7.4 provides the observed filter shifts as seen in calibration data. The given offsets, good to +/- 1 pixel, are measured relative to the position an object would have through the F120M filter.

Table 7.4: Filter Induced Image Shifts Relative to F120M Image (good to +/- 1 pixel)

Filter	x Shift (pixels)	y Shift (pixels)
F120M	=0	=0
F130M	0	0
F140M	0	0
F140W	-1	2
F152M	0	0
F170M	0	0
F165W	1	1
F175W	-1	1
F190M	1	0
F210M	1	0
F220W	-1	2
F231M	1	-3
F253M	-1	3
F275W	-1	2
F278M	-2	4
F307M	-2	5
F320W	-73	46
F342W	-1	-2
F346M	-5	6
F372M	-4	6

Table 7.4: Filter Induced Image Shifts Relative to F120M Image (good to +/- 1 pixel) (Continued)

Filter	x Shift (pixels)	y Shift (pixels)
F410M	-12	17
F430W	1	8
F370LP	0	2
F480LP	-1	1
F486N	-6	16
F501N	11	0
F502M	-1	-7
F600M	24	11
F550M	-1	-5
F1ND	0	0
F2ND	1	0
F4ND	0	-1
F6ND	0	0

7.8 Errors in Absolute Photometry (f/96)

The absolute photometric accuracy of FOC observations depends on several factors. This section will not discuss those sources of error that arise from errors in the flatfield correction and associated effects (e.g., pattern noise). The remaining errors most likely arise from: 1) errors in the published fluxes or variations in fluxes of the spectrophotometric stars used to calibrate the absolute DQE, 2) errors in the assumed PSFs, 3) errors in the assumed filter transmission curves, 4) format dependence effects, 5) temporal variability in the FOC detectors, and 6) the spectrum of the source. This section will summarize the current understanding (or lack thereof) of these errors. As the *f*/48 detector is much more poorly calibrated, it will be discussed separately. For a summary of FOC accuracies, see Figure 8.4.

- ***Errors in the spectrophotometric standards.*** The spectrophotometric standards used for the FOC DQE determination are on the flux scale derived from correcting IUE spectra of the white dwarf G191B2B to conform to the pure hydrogen model of Finley (see Colina and Bohlin, *AJ* 108, 1931 (1994)). The spectra of the standards used here (BPM16274 and HZ4) were corrected using the same function. While it is difficult to assign a formal uncertainty to the predicted filtered fluxes due to errors in the spectrophotometry, assigning an error of +/– 3% is probably conservative enough.
- ***Errors in the assumptions for the PSF.*** Because the in-orbit calibrations relied on large aperture photometry, there should be very little sensitivity to details of the PSF or changes in the PSF. This source of error should con-

tribute less than 1% error to the derived efficiencies. (Note that quite the opposite is true when deriving total fluxes of stars from core-aperture or PSF-fitting photometry techniques).

- ***Errors in the assumed filter transmission curves.*** Although the filter transmission curves were carefully measured on the ground, that does not preclude some sort of subsequent degradation or change in performance. There has been no unambiguous evidence for changes in any particular filter's bandpass. There is some evidence that the redleaks of some filters differ significantly from their published values.
- ***Format dependence.*** A variation of sensitivity with video format has been noted. In particular, Table 7.3 shows the relative response of the more common *f*/96 formats with respect to the 512 x 512 imaging format. These determinations are not known completely accurately. Most of the absolute sensitivity calibration observations used the 256 x 256 format, so the uncertainty in the calibration of the format dependent sensitivity for this format enters into the uncertainty for all the formats. The uncertainty is approximately 3%. No such table has been derived for *f*/48. Note that if the image is calibrated using the PHOTFLAM from the image and the PHOTMODE keyword value indicates the format used, then no re-calculation of the absolute sensitivity is required.
- ***Variability of f/96 DQE.*** The overall throughput of the FOC has been monitored over the three years before the first servicing mission, and in the UV since the servicing mission. The only evidence for change has been an ~3% decline in the sensitivity over three years, independent of wavelength. From the time COSTAR was installed until mid-1996, there was no significant sensitivity change in the ultraviolet, but a slow downward trend of approximately 10% per year has been seen in the UV since then.
- ***Source spectrum.*** The value of PHOTFLAM averages F_λ over the bandpass. Situations where the detected flux distribution is skewed in wavelength can lead to large errors in assigning the absolute sensitivity calibration to the adopted (pivot) wavelength, especially when the wideband filters are being used or where redleak plays a significant part. If there is any doubt as to whether there are significant color effects, observers are advised to use **synphot** or **focsim** to check their absolute fluxes. FOCSIM is an FOC simulator that can be run under IRAF at STScI or from a WWW form found on the FOC world wide web pages. This error is very dependent on the filter being used and the source spectrum, so no rules of thumb about its magnitude can be given.

7.9 Absolute Sensitivity of the f/48 Detector

The DQE of the *f*/48 camera was never calibrated systematically because the existing spectrophotometric standards are generally too bright and the *f*/48 relay has no neutral density (ND) filters to attenuate their fluxes. A calibration program

was developed and run in December 1993, after COSTAR was installed but before it was deployed. The results of this program are presented in *FOC ISR* 077. This study indicated that the sensitivity from about 1800 Å to 3000 Å appears to be about 60% of the prelaunch estimate of sensitivity, with some uncertainty because the data used to derive this factor were less than ideal.

In general, *f*/48 fluxes must be considered quite uncertain. A typical error estimate of +/– 30% is appropriate.

Chapter 8
FOC Data Analysis

In This Chapter...

The FOC is a versatile instrument capable of high-resolution imaging, polarimetry, and both slitless and long-slit spectroscopy. This chapter briefly describes some helpful data analysis techniques and IRAF/STSDAS tasks for reducing FOC data and indicates the kinds of accuracies you can expect.

8.1 Photometry

The basic strategy for performing photometry on FOC point sources proceeds as follows:

- Choose an appropriate aperture size.
- Measure the counts within the aperture.
- Measure the background flux outside the aperture.
- Assess the fraction of encircled signal within your aperture using an appropriate FOC point spread function (PSF).
- Convert counts to flux using the PHOTFLAM keyword and exposure time.

You can easily do the first three steps with standard IRAF aperture photometry tasks, for example, the **phot** task in the **noao.digiphot.apphot** package. Below we describe how to work with FOC point spread functions, and the section on "Converting Counts to Flux or Magnitude" on page 3-15 shows how to use the PHOTFLAM keyword.

8.1.1 Point Spread Function

Users performing photometry on FOC point sources need to know how to normalize their point-spread functions. In other words, given your particular combination of aperture and background annulus sizes, what fraction of the total flux are you measuring? In order to help you answer this question, a set of observed PSFs is publicly available via the WWW at:

`http://www.stsci.edu/ftp/instrument_news/FOC/foc_tools.html#psfs`

Alternatively, you can retrieve the PSFs via anonymous FTP from `ftp.stsci.edu` in the directory:

`/instrument_news/FOC/Foc_tools/psfs/psf_files/f96/foc+costar`

Once you have selected the appropriate PSF for your observed wavelength, you can apply the very same aperture and background annulus parameters to determine the fraction of the total flux that your technique measures.

The on-line PSF files are in FITS format and have been normalized so that the total background-subtracted flux is 1.0. The total fluxes and backgrounds were measured in exactly the same way as the DQE curve. So, for example, if a particular choice of aperture size and background region returns the result of 0.5 when applied to a PSF file, then 50% of the flux is measured.

Another example may further clarify this procedure. The image `x2330106p` is a 596 second F220W image of a field in the globular cluster 47 Tucanae. The inverse sensitivity for this image, given by the keyword PHOTFLAM in the image header, is 2.017×10^{-17}. However, as pointed out in “Absolute Sensitivity Correction (WAVCORR)” on page 6-3, the PHOTFLAM values in data taken in the early part of the COSTAR-corrected era were incorrect in that they did not use the COSTAR element in the PHOTMODE string, and the DQE curve used was subsequently superseded by one made using on-orbit measurements. Using **synphot** to re-evaluate the PHOTFLAM for this mode gives 3.131×10^{-17}. Photometry done on a particular star using **phot** found a total of 631.52 counts with a particular choice of aperture parameters. Using the same choice of parameters on the F220W PSF gives 0.713, or 71.3% of the flux. Thus, the total flux from the star is 631.52 / 0.713 = 885.72 counts, and the total count rate is 885.72/596.0 = 1.486 counts/sec. The weighted mean flux from the star over the F220W+FOC+OTA+COSTAR passband is then $1.486 \times 3.131 \times 10^{-17} = 4.65 \times 10^{-17}$ erg cm^{-2} s^{-1} Å^{-1}.

One troublesome feature of the FOC’s nearly diffraction-limited PSF is that small aberrations can affect the photometry significantly, especially within small apertures. Users should be aware that small, unpredictable, time-dependent focus variations due to thermal effects in the OTA (*breathing*) can slightly defocus the FOC PSF. The effect on photometry is small for aperture radii larger than 0.1 arcseconds (a few percent at most), but the flux in the central pixel can vary by more than a factor of two from one exposure to the next, especially in the 2000 to 3000 Å range.

Unfortunately, there is no good method to determine the quality of the focus for a particular image, making it very difficult to model the effect of defocusing on

the aperture correction for stellar images. The alternative is to increase the sizes of the error bars to account for this uncertainty in the photometric zero point.

Similarly, there is a small field dependence of the PSF, mainly a focus and astigmatism term. The magnitude of the effect is small over the 512 x 512 imaging format compared to, say, the variations due to breathing. However, again there is no way to model the effect since it presupposes knowledge of the focus of the image at the center of the field.

Overall, users are advised to use an aperture larger than 0.1" radius if accuracy in the zero-point is required to better than 5%. Otherwise, one must expect some uncertainty in the zero point due to aperture correction uncertainties.

As already mentioned in Chapter 4, all pre-COSTAR data are affected by the spherical aberration of the primary mirror. This aberration seriously degraded the FOC PSF, which featured a diffraction limited core (~70 milliarcseconds FWHM) containing 10–15% of the total light of the source, superimposed on a bright diffuse halo. Figure 8.1 shows the aberrated PSF of a spectrophotometric standard star taken with the *f*/96 and the F140M filter.

Despite the difference between the PSFs obtained with and without the COSTAR correction, exactly the same considerations apply for determining the aperture correction. The difference is that, instead of measuring PSF flux fractions of 50% or higher, most small apertures will only include 5–20% of the flux when applied to pre-COSTAR PSFs. To enclose 50% of the flux required using an aperture size of 0.6 arcsec or so.

8.1.2 Photometric Accuracy

Several factors affect the accuracy of relative and absolute photometry with the FOC.

- ***Relative Photometry:*** The accuracy to which you can measure the relative fluxes of sources on the same FOC image is dominated by errors in the flat-fielding and is expected theoretically to be of the order of 3–5% for sources that do not fall on recognizable image defects (see "Commonly Observed Features" on page 4-7). Empirical determinations of photometric accuracy show that repeatabilities of 3–4% are typical for isolated bright stars where crowding is not important and the total detected flux is more than about 3000 counts. However, tests of photometric accuracy in crowded fields suggest relative errors of about 5% for *f*/96 and 10% for *f*/48.

  Users should bear in mind that there are no systematic, detailed studies of relative photometry with the FOC, so these estimates of the rms repeatability are somewhat anecdotal.

Figure 8.1: Pre-COSTAR Image of a Star Taken with f/96 Relay and F140M Filter,

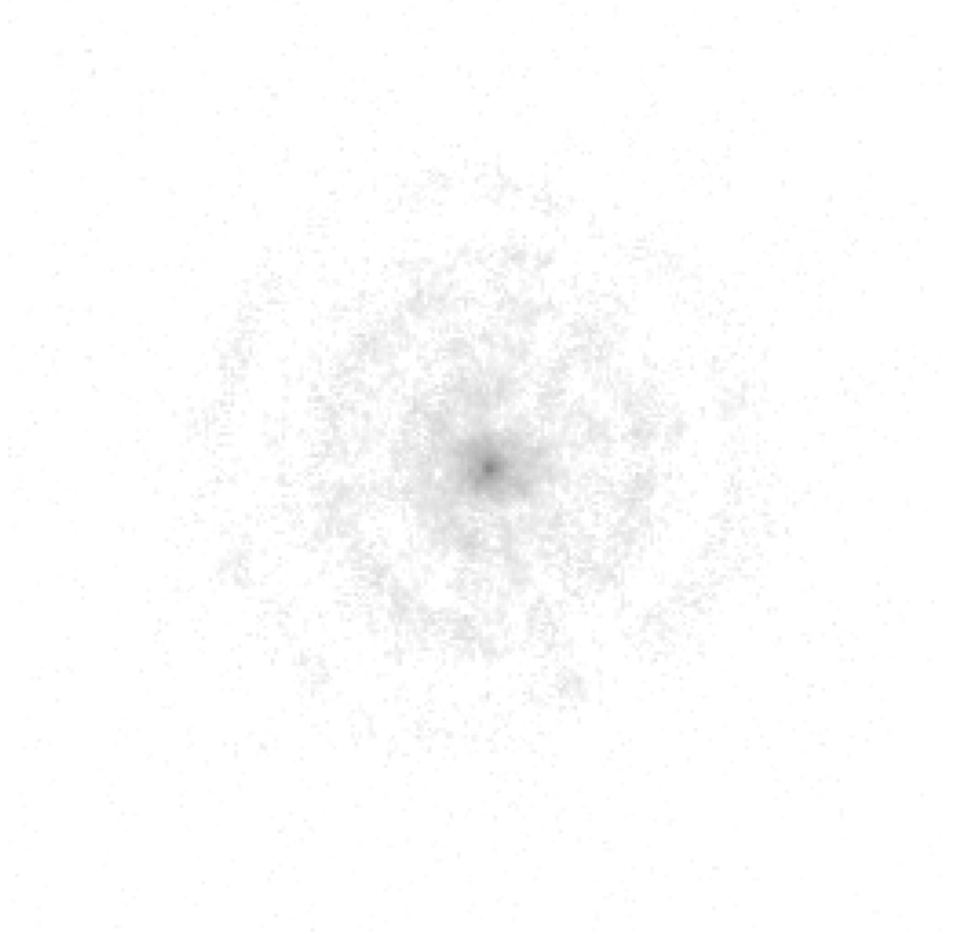

- ***Absolute Photometry:*** The absolute photometric calibration of FOC *f*/96 images was derived empirically by comparing observed and predicted count rates for the spectrophotometric standard stars HZ4 and BPM 16274 (see *FOC ISR* 085). The predicted count rates were calculated using **synphot** from the pre-servicing mission FOC DQE curve, modified to include ground measurements of the COSTAR reflectivity. The observed count rates were measured by summing the flux within an aperture of 70 pixels (1 arcsecond) radius, accounting for the background measured also at 1 arcsecond radius. Note that this procedure is different from the pre-COSTAR case, where a 3 arcsecond radius aperture was used. The measured relation between observed and expected measurements and wavelength was found to be linear, and this linear relation was used to modify the FOC DQE curve. The scatter of the observed and expected measurements using the corrected FOC DQE curve was approximately 8% rms.

The absolute sensitivity of the *f*/48 camera has been calibrated only under conditions of very poor instrument performance (high background), so all *f*/48 fluxes must be considered much more uncertain. Typical uncertainties are of the order of +/- 30%.

Users must also account for the error sources discussed in the previous chapter. In addition to the 10–20% scatter in the absolute calibration accuracy of the *f*/96 camera (and the considerably higher uncertainty in the *f*/48 fluxes), there are several effects that can systematically shift the photometric scale for FOC data and go uncorrected in pipeline processing. These error sources, which should be corrected if possible, include:

- Format dependence of the FOC sensitivities (see page 7-10).
- The effect of the source spectrum on the calculated flux (see page 7-15).
- Flatfielding inaccuracies (see page 7-5 and below)

Accuracy of Flatfielding

Chapter 7 discusses the sources of FOC flatfielding errors at length. Here we summarize their effects on photometric accuracy. The only component of flatfield response currently corrected in the pipeline is that for large-scale variations because the flatfields used have been heavily smoothed. The reasons for the lack of further corrections are as follows:

- Because of the FOC's limited dynamic range, obtaining high signal-to-noise flatfields consumes large numbers of HST orbits. Therefore most flatfields have only a few hundred counts per pixel with a corresponding signal to noise of on the order of 5% per pixel from photon noise alone.
- Small drifts in geometric distortion will shift many of the fine scale scratches and blemishes so that they are no longer aligned with those in the flatfield, producing worse flatfielding results around such features.
- The intensity of scratches and blemishes varies considerably with wavelength in the UV. Because there is a UV flatfield at only one wavelength, its scratches and blemishes will be of the wrong depth for most other images.
- Pattern noise and many of the other fine defects in FOC images are not stable and will not be properly removed.

The resulting accuracy of relative photometry is largely governed by the small scale defects, scan rate oscillations, the intrinsic error in the large scale flatfield, and changes in the flatfield that depend on wavelength. This last error is probably on the order of 2–4% rms (this and subsequent discussions of errors apply to the area of the photocathode more than about 100 pixels away from the edges and corners of the format). Given the intrinsic error in the large scale flatfields, the observer should not expect the net large scale accuracy to be better than 3–5%. Some recent checks on photometric consistency of stars in a crowded field have had actual errors closer to 7%.

Errors due to scan rate variations may be as high as 10–20% (peak). Fortunately these errors are usually confined to the first 100 pixels or so of the scan line. Fine scale features such as reseau marks, scratches, blemishes, and video defects can result in much higher errors for the affected pixels. The best

data-analysis advice regarding these problems is to avoid placing targets near these defects in the first place! It is possible to flatfield out scratches and blemishes with the appropriate registration of the flatfield with the science image. To obtain the UV flatfield, contact the STScI help desk (`help@stsci.edu`). You should keep in mind, however, that no simple offset is likely to register the flatfield with the science image everywhere in the image. Such efforts are easier if you need to correct scratches and blemishes only in a limited area. Furthermore, if the effective wavelength of the target in the science image is much different from that of the flatfield, the scratches and blemishes may not have the same intensity and may not be flatfielded properly.

Pattern noise can produce fluctuations as large as 10% in some pixels (for *f*/96). Fortunately, most analysis techniques average over at least a few pixels, and because the spatial frequencies of these patterns are high, integration over a sizeable aperture reduces their effect significantly. However, they can seriously affect certain image restoration techniques.

8.2 Astrometry

The astrometric accuracy of FOC data depends on two factors. The first is the pointing accuracy of the FOC. The second is the internal geometric accuracy of an FOC image itself, including the correctness of the distortion model, the plate scale, and the image rotation.

- ***Pointing Accuracy***: Positional errors in the HST Guide Star Catalog contribute most of the error in the RA and Dec assigned to the center of an FOC image. Typical 1σ errors in guide-star positions are +/– 0.33 arcsec in the northern hemisphere and +/– 0.5 arcsec in the south. One might expect that the (unknown) proper motions of guide stars in this catalog gradually add to these errors. The accuracy with which HST places a target in the FOC field of view depends in a complex way on the target coordinate uncertainty, the positions of the guide stars in the FGS fields of view, and the alignment of the FOC imaging aperture with respect to the FGS reference frame. This FOC-to-FGS alignment is maintained to better than 0.2’’, and experience with the overall pointing accuracy of the FOC when GASP coordinates are used has shown that 1 sigma error in the absolute pointing is approximately 0.5 arcsecond.

  On top of these errors, different filters induce different target shifts within FOC images (Table 8.1 lists known filter shifts). In most cases, the translation of the image due to the filter is small (1–3 pixels, or 0.015–0.05 arcsec), but some filters do introduce a large shift. Particularly notable are the F320W (shift=88 pixels) and F486N (shift=20 pixels) filters.

- ***Relative Positions:*** The best estimate of the accuracy of the relative positions within an FOC image comes from the rms residuals of star positions in the crowded field used for calibrating the geometric distortion. Typical values are 0.3 pixels (0.005 arcsec) for the 512 (zoomed) x 1024 format and

0.2 pixels (0.003 arcsec) for the 512 x 512 format. These uncertainties are compounded by the uncertainty in the plate scale, which is subject to time variation.

The absolute calibration of the plate scale and rotation has been accomplished in two ways; firstly, by observations of an astrometric star field using astrometric guide stars, and secondly by using the programmed offsets between observations in the crowded-field geometric distortion analysis. Typically, these different measurement methods give consistent results in cases where the pointing system operates without anomalies. However, the FOC plate scale can vary from switch-on to switch-on. Comparisons of images of the same field taken several months apart have shown plate-scale variations as large as 0.7%. These time-dependent drifts of the FOC plate scale have never been studied in any systematic way.

Based on all the above, the best estimate for the *f*/96 plate scale is:

f/96 plate scale = 0.01435 +/- 0.00007 arcseconds/pixel

Recent measurements of the *f*/48 plate scale which compare images of the same crowded field from both the *f*/48 and *f*/96 cameras show that the plate scale of the *f*/48 is:

f/48 plate scale = 0.02870 +/- 0.00029 arcseconds/pixel.

The best estimates for the pre-COSTAR *f*/96 and *f*/48 plate scales are:

f/96 plate scale = 0.02217 +/- 0.00010 arcseconds/pixel
f/48 plate scale = 0.04514 +/- 0.00012 arcseconds/pixel.

8.3 Polarimetry

The *f*/96 camera of the FOC contains three linearly polarizing prisms with names POL0, POL60, and POL120. The *E*-vector pass directions of these prisms are 0 degrees, 60 degrees, and 120 degrees respectively, counterclockwise from the image *x* axis (–S direction), as projected onto the sky. The prisms are birefringent beam splitters that transmit one mode of polarization straight through, while deflecting the orthogonal mode so that it misses the central 512 x 512 region of the photocathode.

The pipeline calibration for polarization observations is no different than for other images. That is, no special correction for polarization is applied, and the images are not combined to form Stokes parameter images.

A polarimeter based on three separate polarizers cannot be expected to yield extremely accurate results. One difficulty is that the throughputs of the three polarizers are not identical, and these differences in throughput depend on wavelength. While the filter transmissions have been measured on the ground, filters do change with time, and color variations in the source will result in small differences in the observed throughput. Variations of order one percent exist throughout the visual wavelength range, but the major difference is that the short-wavelength cutoff of POL60 occurs about 500 Å longward of the cutoff of

POL0 and POL120. This divergence begins at about 3000 Å. Tasks in the **synphot** package can be used to determine the expected throughputs of each of the polarizers together with other filters used for your observations. You can then divide each of the three images by the expected throughput to correct for this difference.

Another limitation of FOC polarimetry is that the incoming light reflects off several mirrors at oblique angles, ranging from a few degrees up to about 11.5 degrees. An oblique reflection at 11.5 off aluminum induces a linear polarization of about 0.2% in incident unpolarized light, and it also results in a phase shift of about one degree. Such a phase shift is insignificant for incident linearly polarized light. If the incident light were 100% circularly polarized, however, a one-degree phase shift would induce a spurious linear polarization of nearly two percent, which would be significant.

Introducing a polarizer into the beam shifts the image by several pixels. The amount of this shift must be known in order to determine the Stokes parameters from the three images. The shifts at various wavelengths are shown in Table 8.1. These values were based primarily on observations with the F346M filter and an objective prism, but observations with F220W and F140W were also used. The wavelength dependence is then derived from the dispersion curve of the far-UV objective prism (FUVOP). With POL0 or POL120 these values are believed to be good to 0.1 or 0.2 pixel, but with POL60 the uncertainty is more like half a pixel because the observations were of lower quality.

Table 8.1: Image Shifts at Various Wavelengths

Wavelength (Å)	POL0		POL60		POL120	
	x	y	x	y	x	y
2500	1.4	-7.3	-2.3	-9.1	1.2	-6.5
3000	1.3	-7.1	-2.2	-8.8	1.2	-6.3
3500	1.3	-7.0	-2.2	-8.7	1.2	-6.2
4000	1.3	-6.9	-2.2	-8.6	1.2	-6.1
4500	1.3	-6.9	-2.2	-8.6	1.2	-6.1
5000	1.3	-6.9	-2.2	-8.5	1.2	-6.1
5500	1.3	-6.8	-2.2	-8.5	1.2	-6.1
6000	1.3	-6.8	-2.1	-8.5	1.2	-6.0

The image quality of the FOC suffers somewhat when a polarizing prism is used. While POL0 and POL120 are not bad, and POL60 seems to be good in the visual and blue range, the optical quality of POL60 deteriorates substantially at the shortest wavelengths that the polarizer passes, around 2200 Å. However, polarization observations at wavelengths shortward of about 3000 Å will be very difficult anyway because of the UV transmission cutoff of POL60.

After correcting for these unequal throughputs and shifting the images to register them, you can compute the Stokes parameters (*I*, *Q*, *U*) by simple arithmetic using the **imcalc** task. Using the **imcalc** notation `im1`, `im2`, and `im3` to represent the images taken through the polarizers POL0, POL60, and POL120 respectively, the Stokes parameters are as follows:

$$I = \frac{2}{3} \times (im1 + im2 + im3)$$

$$U = \frac{2}{\sqrt{3}} \times (im3 - im2)$$

$$Q = \frac{2}{3} \times (2 \times im1 - im2 - im3)$$

These values can be converted to the degree of polarization *P* and the polarization angle θ , measured counterclockwise from the x axis as follows:

$$P = \frac{\sqrt{Q^2 + U^2}}{I}$$

$$\theta = \frac{1}{2}\tan^{-1}\left(\frac{P}{Q}\right)$$

The polarization errors arising from Poisson noise when *N* counts have been gathered in the three polarization image are given by:

$$\sigma_P = \sqrt{\frac{2}{N}}$$

$$\sigma_\theta = \frac{\sigma_P}{2P}$$

Even for very large *N* (i.e. very good signal-to-noise), polarizations of point sources as low as 1–2% are very difficult to detect reliably because the limiting photometric accuracy of the FOC itself is close to this level. Uncertainties in flatfielding, filter transmission uncertainties, PSF differences between polarizers and other effects will conspire to thwart any attempts to measure polarizations to very high accuracy unless great care is taken to try and minimize the instrumental effects (e.g. by dithering the images, dividing into shorter exposures to investigate PSF changes and differences). Flatfield uncertainties and PSF dependences are less of a factor when analyzing extended sources (with sizes larger than 15 pixels or so), so polarization accuracies of 1% or so are probably achievable for extended sources.

8.4 Objective-Prism Spectroscopy

The FOC objective prism facility consists of a far-UV prism and a near-UV prism for both the *f*/96 and *f*/48 cameras. The far-UV prism (FUVOP) operates down to 1150Å with a wavelength dispersion $\lambda/\Delta\lambda$ of around 50. The near-UV prism (NUVOP) transmits only above 1600 Å with a wavelength dispersion $\lambda/\Delta\lambda$ around 100 at 2500Å. Both the FUVOP and the NUVOP disperse the beam in a direction roughly parallel to the decreasing line number direction with angles of approximately 8 degrees and 11 degrees from the –L direction respectively. This dispersion angle can be seen clearly in Figures 8.2 and 8.3 which show *f*/96 images taken with the FUVOP and the NUVOP respectively. In the NUVOP image, the feature cutting across the spectrum near the top of the image is a blemish in the camera and not an feature in the source.

Figure 8.2: Composite f/96 Image of Undispersed Star and FUVOP Image

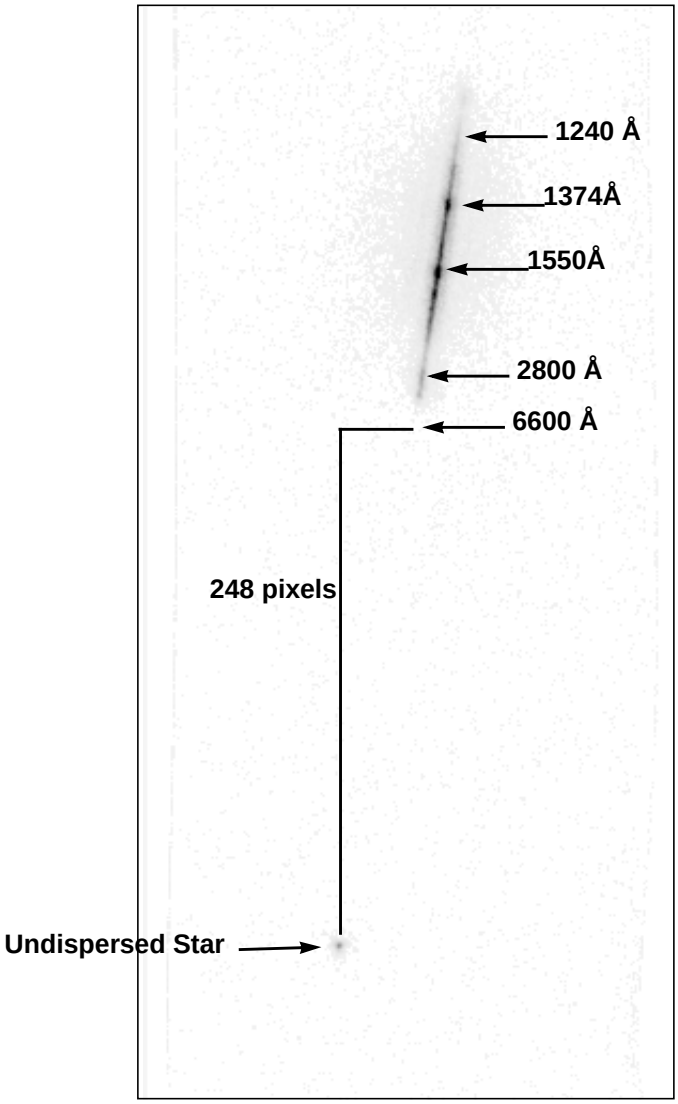

Figure 8.3: f/96 NUVOP Image of Emission Line Source, 256x1024 Format

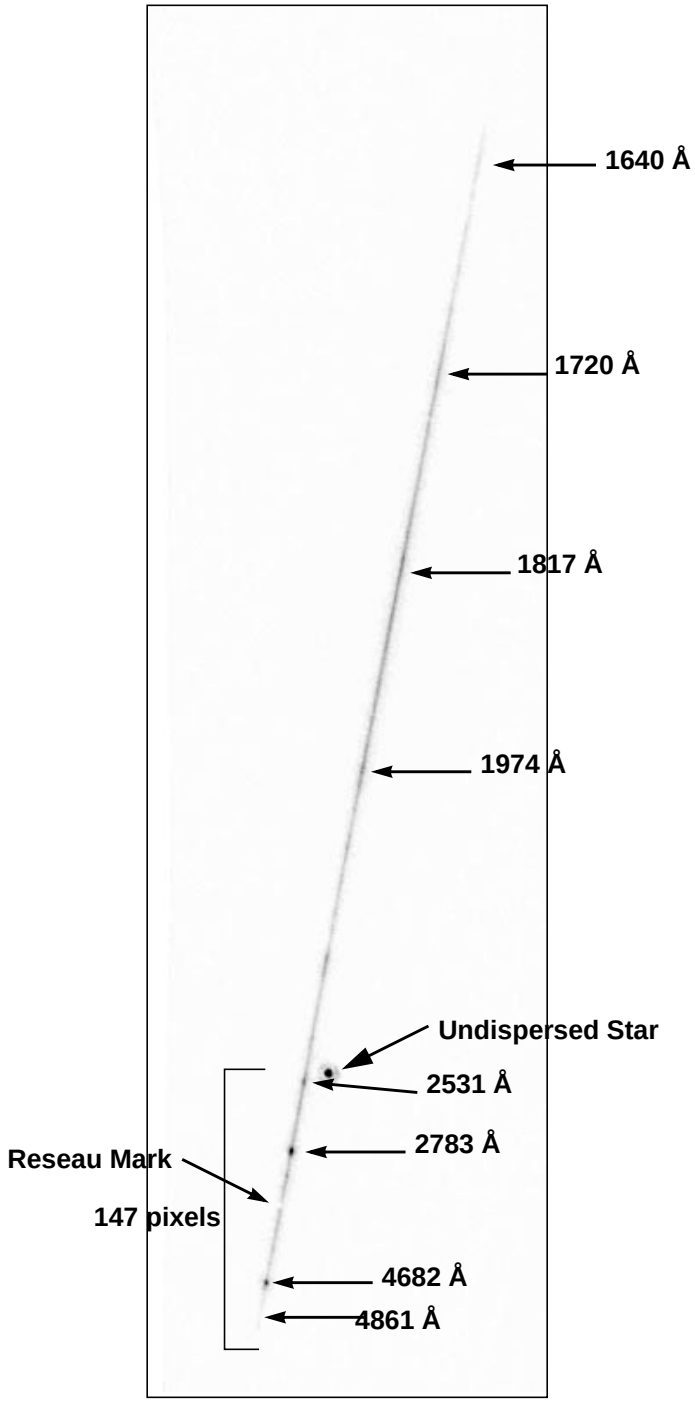

The most recently determined dispersion curves for the *f*/96 objective prisms are given in Table 8.2 along with the available *f*/48 dispersion curves. The wavelengths determined from objective prism spectra using these dispersion curves should have a $\Delta\lambda/\lambda$ error of <1% for *f*/96 spectra. The *f*/48 dispersion curves are based on pre-launch measurements, so their accuracies are uncertain.

The spectral features in Figures 8.2 and 8.3 have been labeled to illustrate the non-linear wavelength dispersion of the prisms.

Table 8.2: FOC Dispersion Curves

f/96 FUVOP		f/96 NUVOP		f/48 FUVOP		f/48 NUVOP	
λ(Å)	Offset	λ(Å)	Offset	λ(Å)	Offset	λ(Å)	Offset
1150	-449.2	1600	-570.1	1100	-248.	1600	-136.0
1200	-416.0	1700	-425.1	1200	-219.0	1700	-109.6
1300	-369.1	1900	-233.4	1300	-189.8	1850	-70.0
1400	-339.2	2100	-122.0	1500	-164.9	1900	-56.8
1600	-306.1	2300	-52.7	1700	-154.0	2000	-36.8
1800	-289.6	2500	-6.3	1900	-147.7	2200	-20.0
2000	-279.6	2700	27.0	2100	-143.5	2500	-1.2
2200	-272.7	2800	40.4	2500	-138.3	2700	6.13
2500	-265.1	3000	62.4	3000	-134.8	3000	14.4
3000	-257.8	3200	79.6	3500	-132.8	3500	23.6
4000	-251.5	3400	93.2	4000	-131.6	4000	29.2
5000	-249.3	4000	120.9	5000	-130.4	5000	35.2
6000	-248.4	5000	145.4	6000	-129.6	6000	41.2
6600	-248.0	6000	158.5	10000	-126.4	10000	65.2

Figure 8.2 shows that *f*/96 FUVOP spectra are only about 175 pixels in length at most, while Figure 8.3 shows that NUVOP spectra are over 650 pixels long. Spectra in typical *f*/48 objective prism images are roughly one half the length of their *f*/96 counterparts. The small PSF cores, only about 3 pixels FWHM, produce only minimal wavelength contamination along the spectra, except in heavily exposed regions of the spectrum, resulting in well-resolved emission lines. The objective prisms can also be used in conjunction with a variety of other filters to isolate particular regions of interest in a source's spectrum.

Several STSDAS tasks have been developed for reduction of FOC objective-prism spectra. These tasks are available as part of the STSDAS **foc.focprism** package but first require the extraction of the spectrum from the image, a procedure handled especially well by the **apall** task in the **noao.twodspec** package. (*FOC ISR 092* provides a tutorial.) Once a one-dimensional version of the spectrum has been extracted from the image, the tasks in the **foc.focprism** package can be used to convert it into flux units.

The task **objcalib** in the **foc.focprism** package uses routines provided by the FOC Instrument Development Team (IDT) to reduce the spectra extracted from objective prism images. It first takes the extracted one-dimensional spectrum given as counts vs. pixels (as produced by **apall**) and applies a dispersion curve to

produce counts vs. wavelength. This step depends on having a reliable dispersion curve to resample the spectrum properly. The task then resamples the spectrum into wavelength bins, and applies a photometric conversion based on the observing mode to convert the counts to physical units ergs cm^{-2} sec^{-1} $Å^{-1}$.

Accurate conversion of the observed counts into flux units relies on knowing the fraction of total emission extracted from the image. Several observations of spectrophotometric standard stars were used to determine this percentage for several given extraction widths, with the results given in Table 8.3. This factor is used to calculate the total flux observed in the spectrum in units of ergs cm^{-2} sec^{-1} $Å^{-1}$. The 3σ errors in the determination of these percentages are also provided as a guide to the expected errors in the resultant photometry. This method assumes that the percentage of light counted in each pixel is the same along the spectrum. Unfortunately, PSFs vary considerably from one end of the spectrum to the other, possibly introducing errors on the order of 10% in the photometry of the spectrum at any given wavelength for *f*/96 spectra. These errors arise from the differences in the encircled energy from one end of the spectrum to the other.

Table 8.3: Photometry for Different Extraction Widths from Objective Prism Spectra (given as a percent of total detected light in the spectrum)

Extraction Width (pixels)	NUVOP		FUVOP	
	ε (%)	3σ error	ε (%)	3σ error
5	55.4	7.4	48.0	8.0
7	62.7	6.9	55.7	7.9
9	68.0	6.5	61.6	7.3
11	72.0	5.9	66.0	5.8

Overall, photometry of objective prism spectra should have errors of about 10% or less for wavelengths below 4000Å for NUVOP spectra and below 2500Å for FUVOP spectra, provided that the position of the undispersed target is known to within a pixel.

8.5 Long-Slit Spectroscopy

The *f*/48 camera of the FOC is equipped with a long-slit spectroscopy facility. Its entrance aperture has a 0.063 x 12.5 arcsecond slit that can be placed at the OTA tangential focus as shown in Figure 9 of the *FOC Instrument Handbook*, version 7.0. The effective wavelength range of this device in first order is 3600–5400Å, in second 1800–2700Å, in third 1200–1800Å, and in fourth 900–1350Å. The MgF_2 window of the detector limits this last range to 1150–1350Å. The linear dispersion at the photocathode is 71, 36, 24, and 18 Å mm^{-1} for the respective orders, and the FOC spectrograph resolution is limited by the slit size and the OTA point spread function to about two to three 24 micron

pixels. Using the Rayleigh resolution criterion, the actual resolving power of the instrument is ~1150 in all orders, yielding spectral resolutions of 4, 2, 1.3, and 1 Å for first, second, third, and fourth orders respectively.

8.5.1 Tribulations of the f/48 Spectrograph

Because of HST's spherical aberration, the long-slit facility was rarely used before COSTAR. In addition, a failure of the *f*/48 camera occurred in September 1992. The high voltage tripped while ramping up at the beginning of an observing sequence. For several years thereafter, the background in the *f*/48 camera was extremely high. As a consequence, the *f*/48 was unavailable to GOs during Cycles 4 and 5 while tests were carried out to establish its performance and operational reliability.

After a long period of inactivity, the *f*/48 was switched on again in November 1994, for the first time after the COSTAR deployment. Images and spectra of an extended target were successfully obtained, although they contained two zones of particularly high background that faded with time, a region in the center known as the *flare* and an *arc* across the top. The locations of these features can be seen in Figure 8.4, where the images from this observing sequence are displayed with the same intensity contrast to allow direct visual comparison. Because the background had finally decreased to manageable levels, the *f*/48 camera was made available to observers in Cycles 6 and 7, limited to *long slit spectroscopy only.* Since then, the prominence of the arc and flare have continued to diminish.

Figure 8.4: .Mosaic of f/48 Images from the November 1994 Test. Time since Switch-on increases from left to right.

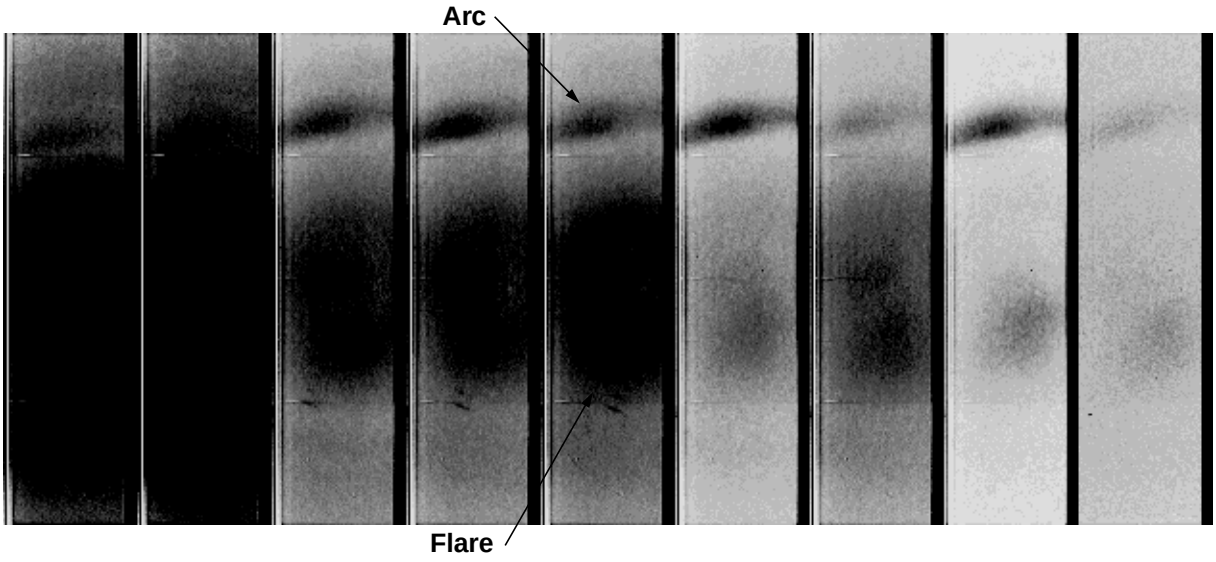

8.5.2 Reduction of f/48 Spectra

FOC long-slit spectra that have undergone geometric correction and wavelength calibration can be reduced with any IRAF task suitable for two-dimensional spectra, such as the **apall** task in the **noao.twodspec.apextract** package. The standard geometric correction procedure remaps the image so that the spectral dispersion runs directly along the *y* axis and the spatial dimension runs along the *x* axis. Corrected spectra have a dispersion of 1.7 Å pixel^{-1}, shifted so that 5300 Å corresponds to *y* pixel 200. Calibration files that simultaneously correct distortion and calibrate the wavelength scale for the 512 zoomed x 1024, 512 x 1024, and 256 x 1024 formats are available through the STScI help desk (`help@stsci.edu`).

Because the standard geometric correction and wavelength calibration procedure does not account for temporal changes in the distortion of the *f*/48 camera, we recommend that you create your own custom geometric correction files, if contemporaneous *f*/48 flatfield observations are available. These internal flatfield images display the reseau marks that trace the geometry of the detector. The transformation that maps these marks to the fiducial positions they would have in a properly corrected image also transforms a contemporaneous raw spectral image into a geometrically-corrected, wavelength-calibrated spectral image. FOC *ISRs* 096 and 097 describe how to generate custom geometric correction files.

The standard spectrophotometric calibration (SDE) file for *f*/48 spectral images presumes that the target is centered in the 0.06” slit, an assumption that is not always valid. Multiplying your geometrically corrected image by the appropriate SDE file for the observing format will convert counts to erg cm^{-2} A^{-1}, correcting for the vignetting of the slit as described in FOC *Instrument Science Report* 098. Integrating the spectrum over the spatial dimension and dividing by the exposure time would then yield a spectrophotometrically calibrated spectrum of a centered point source. To obtain calibrated spectra of extended sources, you will need to multiply by an additional factor of 0.6, because the standard calibration algorithm, geared towards centered point sources, assumes that only 60% of the PSF falls onto the slit.

8.5.3 Accuracy of f/48 Spectroscopy

A calibration program performed in support of the post-COSTAR *f*/48 spectroscopic observations has determined the slit position, geometric distortion, wavelength scale, and spectrophotometric sensitivity of the spectroscopic facility.

- ***Slit Position***: FOC long-slit spectroscopy requires an interactive acquisition, and the position of the slit relative to the target position in an acquisition image is now known to better than 0.1”. However, not all spectroscopic targets in the Archive have been perfectly centered on the slit.

  It is difficult to tell whether a target is centered in an individual spectroscopic image. If the image is part of a series that scans the slit across the target, you can evaluate the location of the target relative to the slit by measuring how the overall spectral intensity varies from image to image.

Otherwise, you can reconstruct, in principle, the relative positions of the target and the slit from the interactive acquisition image, the slew information in the OCX file, and the geometric distortion model of the *f*/48 camera. However, no systematic procedure exists for performing this reconstruction.

- ***Geometric Distortion:*** The geometric corrections for the *f*/48 imaging mode and the *f*/48 spectrographic mode have been determined separately. The distortion model for the imaging mode used for interactive acquisitions relies on the same crowded-field technique as the *f*/96 model. This correction, described in FOC *Instrument Science Report* 095, rectifies the imaging format to 0.5 pixels rms.
- ***Wavelength Calibration:*** Long-slit observations of the planetary nebula NGC 6543 form the basis of the geometric correction and wavelength calibration of the *f*/48 spectrographic mode (see FOC *Instrument Science Reports* 096 and 097.) The resulting transformation rectifies the spectra so that the dispersion direction aligns to within 0.2 degrees of the image *y* axis and the wavelength scale remains stable to within 0.5 Å across the *x* axis. Observers should bear in mind, however, that the geometric distortion of the *f*/48 camera is time-dependent at somewhat less than the 1% level, so custom geometric corrections are necessary to achieve these accuracies.
- ***Spectrophotometric Calibration:*** Above and beyond the difficult-to-measure uncertainties stemming from the placement of the target on the tiny FOC slit, there are other uncertainties with *f*/48 spectrophotometry. Dwell scans of the spectrophotometric standard star LDS 749B, taken as part of the *f*/48 calibration program, yielded one image in which the target fell directly in the center of the slit. The calibration of the FOC's spectrographic throughput rests on this one observation. Comparisons of the resulting sensitivity with the predictions from **synphot** show that the *f*/48 spectrograph is 10% more sensitive than expected at 4000 Å and about 50% less sensitive than expected at 5000 Å. We estimate that these direct sensitivity measurements are correct to about 20%.

  Similar observations of LDS 749B at other scan positions show that the throughput drops by half at an offset of 0.04 arcsec and by 80% at an offset of 0.08 arcsec, so inaccuracies in the target position are likely to be the greatest source of spectrophotometric uncertainty. Furthermore, the wavelength dependence of the off-center throughputs is rather unexpected, being higher in the blue than in the red (see FOC *Instrument Science Report* 098 for more details.)

8.6 Summary of FOC Accuracies

The following table summarizes the kinds of accuracies you can expect when analyzing FOC data. Note that many of these numbers come with qualifications and that you should check the relevant sections of this handbook for details.

.

Table 8.4: Final Accuracies Expected in FOC Observations

Procedure	Estimated Accuracy	Notes
	Calibration (flatfielding)	
Flatfielding	<5% rms large scale	
	5-10% rms small scale	"Clean" areas
	Up to 90%	On reseau marks, scratches
Geometric Correction - *f*/96	0.3 pixel rms	
Geometric Correction - *f*/48	0.5 pixel rms	Full format, central area only.
	Relative photometry (f/96 only)	
Repeatability:	~2-3% rms	As long as statistical errors are not important, target in same place on detector.
Background determination	~1-2%	Depends on aperture size, but generally not a dominant contributor to overall error.
PSF/focus effects, small apertures	Up to 50%	1 pixel aperture, UV wavelengths.
PSF/focus effects, large apertures	~2-3%	Aperture size >10 pixels radius
	Absolute photometry	
Sensitivity - *f*/96	~6% rms for most filters	
	~10% rms for uncalibrated filters	
Sensitivity - *f*/48	~30% for most filters	
	Astrometry	
Relative	0.005" rms (after geometric correction)	
Absolute	1" rms (estimated)	
	Spectroscopy (f/48 only)	
Wavelength Calibration	~0.5-1 Angstrom rms	First order only - higher orders not calibrated.
Spectrophotometry	~10% rms	First order
	~30% rms	Higher orders